ADVANCED ENERGY MATERIALS

Supporting Information

for *Adv. Energy Mater.,* DOI: 10.1002/aenm.202202868

Suppressing Interfacial Recombination with a Strong-Interaction Surface Modulator for Efficient Inverted Perovskite Solar Cells

Bowei Li, Jun Deng, Joel A. Smith, Pietro Caprioglio, Kangyu Ji, Deying Luo, James D. McGettrick, K. D. G. Imalka Jayawardena, Rachel C. Kilbride, Aobo Ren, Steven Hinder, Jinxin Bi, Thomas Webb, Igor Marko, Xueping Liu, Yuren Xiang, Josh Reding, Hui Li, Shixuan Du, David G. Lidzey, Samuel D. Stranks, Trystan Watson, Stephen Sweeney, Henry J. Snaith, S. Ravi P. Silva, and Wei Zhang**

Supporting Information

Suppressing Interfacial Recombination with a Strong-Interaction Surface Modulator for Efficient Inverted Perovskite Solar Cells

Bowei Li, Jun Deng, Joel A. Smith, Pietro Caprioglio, Kangyu Ji, Deying Luo, James D. McGettrick, K. D. G. Imalka Jayawardena, Rachel C. Kilbride, Aobo Ren, Steven Hinder, Jinxin Bi, Thomas Webb, Igor Marko, Xueping Liu, Yuren Xiang, Josh Reding, Hui Li, Shixuan Du, David G. Lidzey, Samuel D. Stranks, Trystan Watson, Stephen Sweeney, Henry J. Snaith, S. Ravi P. Silva, Wei Zhang**

Dr. B. Li, Dr. K. D. G. I. Jayawardena, Dr. Y. Xiang, Dr. A. Ren, Dr. J. Reding, J. Bi, T. Webb, X. Liu, Prof. H. Li, Prof. S. R. P. Silva, Dr. W. Zhang
Advanced Technology Institute, Department of Electrical and Electronic Engineering, University of Surrey, Guildford GU2 7XH, UK
E-mail: wz0003@surrey.ac.uk; s.silva@surrey.ac.uk

Dr. J. Deng, Prof. H. Li, Prof. S. Du
Beijing National Laboratory for Condensed Matter Physics,
Institute of Physics, Chinese Academy of Sciences, Beijing 100190, China

Dr. J. A. Smith, Dr. P. Caprioglio, Prof. H. J. Snaith
Clarendon Laboratory, Department of Physics,
University of Oxford, Oxford OX1 3PU, UK

K. Ji, Prof. S. D. Stranks
Cavendish Laboratory
University of Cambridge, Cambridge, CB3 0HE UK

Prof. S. D. Stranks
Department of Chemical Engineering and Biotechnology,
University of Cambridge, Cambridge CB3 0AS, UK

Dr. J. D. McGettrick, Prof. T. Watson
SPECIFIC, College of Engineering, Swansea University, Swansea SA1 8EN

Dr. R. C. Kilbride
Department of Chemistry
University of Sheffield, Sheffield S3 7HF, UK

Dr. D. Luo
Department of Materials Science and Engineering,
University of Toronto, Toronto M5G 3E4, Canada

Dr. S. Hinder
The Surface Analysis Laboratory, Department of Mechanical Engineering Sciences,

University of Surrey, Guildford GU2 7XH, UK

Dr. I. Marko, Prof. S. J. Sweeney
Advanced Technology Institute, Department of Physics,
University of Surrey, Guildford GU2 7XH, UK

Dr. A. Ren
Institute of Fundamental and Frontier Sciences,
University of Electronic Science and Technology of China, Chengdu 610054, China

Prof. D. G. Lidzey
Department of Physics and Astronomy,
University of Sheffield, Sheffield S3 7RH, UK

This Supporting Information includes:

Experimental Section

Materials

Pre-patterned indium tin oxide (ITO) glass substrates (20 × 20 × 1.1 mm, three-fifths etched ITO) were purchased from South China Science & Technology Co., Ltd. The thickness of ITO is 135 nm and the sheet resistance is around 15 (ohm sq^{-1}). The average transmittance of glass/ITO in the visible region is 88.3%. For chemicals, all of them were purchased from commercial suppliers and used as received. Poly-TPD was purchased from 1-Material. Lead diiodide (PbI_2, 99.99%), lead dibromide ($PbBr_2$,99%) and [2-(9H-Carbazol-9-yl)ethyl]phosphonic acid (2PACz) were purchased from Tokyo Chemical Industry Co., Ltd. (TCI, Japan). Formamidinium iodide (FAI), methylammonium iodide (MAI), 4-Hydroxyphenethylammonium iodide (HO-PEAI) and 2-Thiopheneethylammonium iodide (2-TEAI) were purchased from Greatcell Solar Materials Pty Ltd. *N*,*N*-dimethylformamide (DMF, 99.8%), dimethyl sulfoxide (DMSO, 99.7%), chlorobenzene (CB, 99.8%), and toluene (99.85%) were purchased from Acros. Cesium iodide (CsI, 99.999%), isopropanol (IPA, 99.5%) and methanol (99.8%) were purchased from Sigma-Aldrich. $PC_{61}BM$ (99.5%) was purchased from Solenne. Bathocuproin (BCP, 98%) was purchased from Alfa Aesar. F4TCNQ was purchased from Xi'an Polymer Light Technology Corp. (China).

Methods

***Hole transport layer*.** Poly-TPD solution contains 1 mg mL^{-1} poly-TPD and 0.2 mg mL^{-1} F4-TCNQ. These two chemicals were dissolved in toluene separately and then mixed in the same vial. The mixed solution was stirred at room temperature overnight and filtered with 0.2 μm PTFE before use. ITO substrates were cleaned by ultrasonication with detergent, deionized water, acetone and isopropanol (IPA), followed by 10 min O_2 plasma and then transferred into a N_2-filled glove box. To

prepare the hole transport layer, 60 μL poly-TPD solution was dropped on the cleaned ITO and then spin-coated at a speed of 2000 rpm (2000 rpm s^{-1}) for 30 s. Thereafter, the substrates were annealed at 130 °C for 10 min. Before depositing perovskite, the poly-TPD film was prewetted by different concentrations of 2PACz ranging from 0.25 mg mL^{-1} to 2 mg mL^{-1} at the same program for 30 s and then annealed at 130 °C for 5 min.

Perovskite film. Perovskite precursor is optimized based on the previous report.[1] Herein, the PbI_2, $PbBr_2$, FAI, MAI, CsI were mixed and dissolved in 1 mL DMF:DMSO (4:1 V/V). The stoichiometric ratio is $Cs_{0.05}FA_{0.79}MA_{0.16}PbBr_{0.6}I_{2.4}$ without excess composition. The prepared solution was stirred at room temperature overnight before use. For perovskite film deposition, 60 μL precursor was dropped and spread evenly by pipette tips on the modified poly-TPD. Then, the solution was spin-coated by a two-consecutive step program at 1000 rpm (200 rpm s^{-1}) for 10 s and 6000 rpm (1000 rpm s^{-1}) for 35 s. During the second step, the film was quickly washed by 100 μL CB at 5 s before the end of the program. Subsequently, the samples were annealed on a hotplate at 90 °C for 80 min. After that, there is no extra annealing process in the following steps. To obtain a high-quality perovskite film, the temperature in the glove box should be less than 30 °C (25 ~ 29°C for our normal preparation). In addition, the glove box is regenerated every three months. For the passivation layer, HO-PEAI and 2-TEAI solution (0.5 to 5 mg dissolved in 1 mL IPA) was dynamically spin-coated on the perovskite surface at 5000 rpm (2500 rpm s^{-1}) for 30 s.

Electron transport layer and metal electrodes. PCBM solution contains 30 mg mL^{-1} $PC_{61}BM$ in chlorobenzene. The PCBM solution was stirred at 60 °C for 2 h and filtered through 0.2 μm PTFE before use. BCP solution contains 0.5 mg mL^{-1} BCP in

IPA, which was stirred at a high temperature until dissolved and filtered with 0.2 μm PTFE before use. To prepare the electron transport layer, 60 μL PCBM solution was dynamically spin-coated on top of perovskite film or passivated perovskite film at 2500 rpm (2500 rpm s^{-1}) for 30 s. Then, BCP solution was dropped on the substrate and spin-coated at 5000 rpm (850 rpm s^{-1}) for 25 s. Finally, 100 nm of Ag back electrode was thermally evaporated under a high vacuum (< 3×10^{-6} mbar). A shadow mask was used to pattern the electrodes and the active area is ~ 0.25 cm^2.

Characterization

J-V curves. To ensure accuracy, a mask with an aperture area of 0.09 cm^2 was employed during the measuring process. The *J-V* and SPO measurements were performed outside the glove box by using a Keysight B2901A Source Meter under simulated one-sun AM 1.5G illumination (100 mW cm^{-2}) based on a AAA steady solar simulator (Enlitech, SS-F5-3A). Before each measurement, the simulator was cautiously calibrated by using a standard monocrystalline silicon solar cell with a KG-5 filter same as previously reported,[2] and a double-check reference cell purchased from Fraunhofer ISE CalLab (ISE001/013-2018). All devices were measured both in a reverse (1.2 → − 0.2 V, step 0.02 V, delay time 100 ms) and forward scan (− 0.2 → 1.2 V, step 0.02 V, delay time 100 ms). The *J-V* curve only scanned once for all the devices. For stabilized PCE, the device was measured under the same condition at the maximum power output bias voltage (V_{MAX} or V_{MPP}). All the data were collected by the IV testing system with the software (IVS-KA5000). For stabilized V_{OC}, the device was measured at 0 A to simulate the open-circuit condition under the one-sun AM 1.5G illumination (100 mW cm^{-2}) and the data were collected by using Keysight B2900 quick *IV* measurement software.

External quantum efficiency (EQE) spectrum. EQE was measured outside the glove box by a commercial system (Bentham PV300). The monochromatic light intensity was calibrated by a traceable silicon reference detector (300 – 1100 nm) from the national metrology institute (NMI). For each device, a 0.16 cm^2 mask was used during the measurement to ensure the probing beam (size is 2.2 mm × 2.2 mm) fully inside the electrode area.

Scanning electron microscopy (SEM). The SEM images were obtained from Jeol 7100F. The cross-sectional SEM image was conducted by carefully fracturing the device vertically.

Contact angle. The contact angles were measured using a contact angle analyzer (Drop shape analyzer-DSA25, KRŰSS GmbH). 2 μL DI water was dropped on the perovskite samples and measured in the air under room temperature.

Ultraviolet-visible (UV-Vis) absorption spectra. The absorption spectra were performed by Varian Cary 5000 UV-vis-NIR spectrophotometer.

Electrochemical impedance spectroscopy (EIS). The EIS measurements were performed by Gamry Interface 1000 in the frequency from 1 MHz to 1 Hz at a bias of 0.5 V under dark.

X-ray Photoelectron Spectroscopy (XPS). XPS spectra were acquired on a ThermoFisher Scientific Instruments (East Grinstead, UK) K-Alpha$^+$ spectrometer. XPS spectra were acquired using a monochromated Al Kα X-ray source (hν = 1486.6 eV). An X-ray spot of ~200 μm radius was employed. Survey spectra were acquired employing a Pass Energy of 200 eV. High resolution, core level spectra were acquired with a Pass Energy of 50 eV and a step size of 0.1 eV. Quantitative surface chemical analyses were calculated from the high resolution, core level spectra following the removal of a non-linear (Shirley) background. The Avantage software was used which

incorporates the appropriate sensitivity factors and corrects for the electron energy analyzer transmission function. All spectra were charge referenced against the C1s peak at 285 eV to correct for any charging effects during data acquisition.

Ultra-violet photoelectron spectroscopy (UPS). UPS was carried out on a Kratos Axis Supra XPS Spectrometer (Manchester, UK) using a He(I) plasma source (hν = 21.22 eV). A 110 µm aperture was used to limit the analysis area and spectra were collected with a pass energy of 10 eV and a step size of 0.05 eV. A bias of 9.0 V was applied to the samples and the integral charge neutraliser was disabled. C(1s) XPS spectra were collected in situ to confirm no charging effects, and the UPS spectra have no charge correction applied. The secondary electron cutoff & valence band maximum are estimated at the x-axis intercept using the „Step Up“ and „Step Down“ backgrounds respectively in CasaXPS Version 2.3.24PR1.0 (Teignmouth, UK).

Transient photovoltage (TPV). TPV measurements were conducted as in our previous report.[3]

Electroluminescence (EL) and External quantum efficiency of electroluminescence (*EQE_{EL}*). All the EL and EQE_{EL} measurements were carried out based on unencapsulated devices at room temperature in ambient air. A Keithley 2400 Source Meter was used to apply a DC bias. The EL emission spectra were measured using an Ocean Optics HR2000+ fiber-coupled spectrometer. The radiant power of the devices was measured by a ILX Lightwave OMM-6810B optical multimeter with a calibrated silicon power head centered over the device pixel.[4] The EQE_{EL} was calculated from the radiant power, current density and EL emission spectrum, and a Lambertian profile was assumed in the calculation.

X-ray diffraction (XRD). Samples for XRD were prepared as per the device fabrication, finishing after the perovskite (or post-treatment) layer. XRD patterns were

measured using a Panalytical X'Pert Pro diffractometer in reflection geometry using a Cu anode source (Cu Kα radiation, λ = 1.506 Å).

Grazing-incidence wide-angle X-ray scattering (GIWAXS). GIWAXS was performed using a lab-based Xenocs Xeuss 2.0 system combining a Ga MetalJet source (Excillum) with a Pilatus3R 1M hybrid photon counting (HPC) detector (Dectris). X-ray photons with energy 9.243 keV (λ = 1.341 Å) were directed towards an aligned sample surface held at a grazing incidence angle of 0.3° which was calculated to give an attenuation length of 50 nm into the film.[5] Scattered X-rays were collected by the 2D HPC detector, which was positioned ~0.3 m from the sample, with the sample chamber, detector and flight tube held at vacuum during measurement to prevent air scattering. The alignment was calibrated using AgBe, and the 2D data was integrated and reshaped using scripts based on the PyFAI and pygix libraries.[6]

Carrier lifetime mapping. The carrier lifetime mapping was conducted using a confocal microscope setup (MicroTime-200, PicoQuant, Germany). The sample was excited by a 405-nm pulsed diode (PDL 828 -S"SEPIA II", PicoQuant, pulse width ~ 100 ps) with an air objective. The signals were focused onto a Hybrid PMT detector connected to a Picoquant acquisition card for time-correlated single-photon counting (time resolution of 200 ps). An incident power of 80 nW was used which corresponds to a fluence of 1 μJ cm^{-2}.

Photoluminescence quantum yield (PLQY): The absolute photoluminescent measurements were measured by exciting the sample with a CW laser source of 532 nm (ThorLabs DJ532-10) at 1 sun intensity equivalent inside an integrating sphere. All spectra are illuminated for the same amount of time of 5 s in order to improve

consistency. The actual photoluminescence spectra are recorded through a Maya2000 Pro spectrometer by using Ocean View software.

Computational methods. The first-principles calculations were carried out with the density functional theory (DFT) implemented in the Vienna ab initio simulation package (VASP).[7] We adopted the generalized gradient approximation (GGA) in the form of the Perdew-Burke-Ernzerhof (PBE)[8] for the exchange-correlation potentials. The projector augmented-wave (PAW)[9] pseudopotentials were used with a plane wave energy of 500 eV. A Monkhost-Pack[10] Brillouin zone sampling grid with a resolution of $0.02\times2\pi$ $Å^{-1}$ was applied and atomic positions and lattice parameters were relaxed until all the forces on the atoms were less than 5×10^{-2} eV/Å for bulk $FAPbI_3$. To simulate the adsorption of TEAI and HO-PEAI on the $FAPbI_3$, we built a 3×3×2 superlattice of PbI_2-terminated surface, where the vacuum layer of 20 Å was used to avoid the interlayer interactions along the c direction. Considering the large number of atoms in the model, only Γ point was used in the Brillouin zone sampling and atomic positions were relaxed until all the forces were less than 5×10^{-2} eV/Å. Note that we only relaxed the upmost Pb-I layer and the 2-TEAI/HO-PEAI molecule, while keeping the bottom atoms fixed. The adsorption energy was calculated with the following equation:

$$\Delta E_{ads}=E_{system}-E_{slab}-E_{molecule} \quad \text{(S1)}$$

where E_{system} is the total energy of the model, E_{slab} the total energy of $FAPbI_3$ slab, and $E_{molecule}$ total energy of the molecule.

The charge density difference was obtained by $\Delta\rho=\rho_{system}-\rho_{slab}-\rho_{molecule}$, where ρ_{system} is the charge density of the model, ρ_{slab} the charge density of $FAPbI_3$ slab, and $\rho_{molecule}$ the charge density of the molecule.

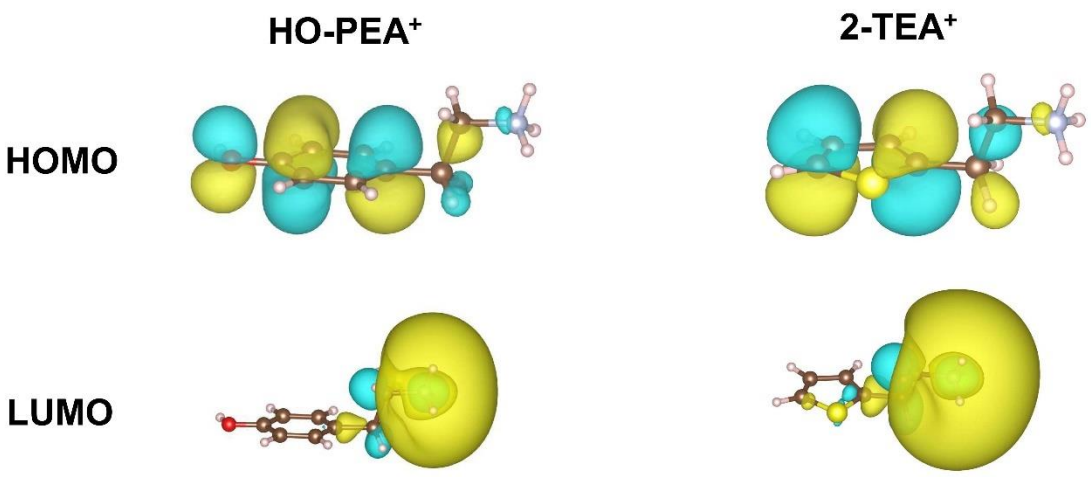

Figure S1. Highest occupied molecular orbital (HOMO) and lowest unoccupied molecular orbital (LUMO) of HO-PEA$^+$ and 2-TEA$^+$.

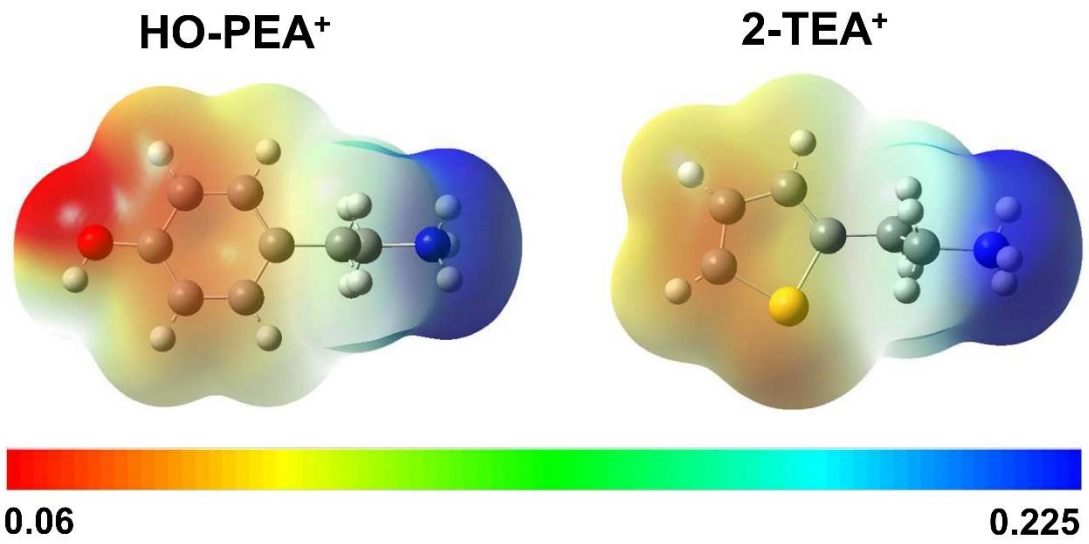

Figure S2. The electrostatic potential (ESP) maps of HO-PEA$^+$ and 2-TEA$^+$. The ESP was calculated by using the Gaussian 09 program package with B3LYP/6–31G* basis.

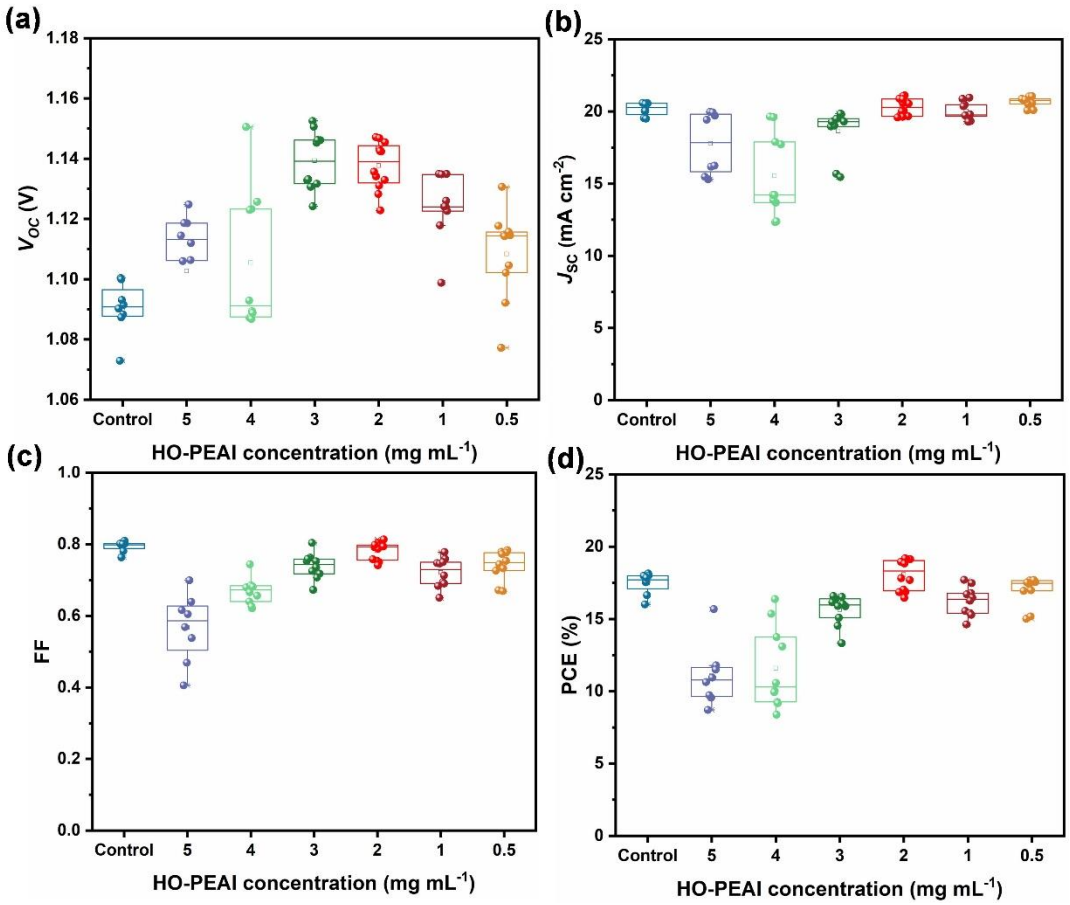

Figure S3. Statistical distributions of photovoltaic parameters (V_{OC}, J_{SC}, FF and PCE) based on the different concentrations of HO-PEAI. The devices with the structure of glass/ITO/poly-TPD/PFN-Br/perovskite/HO-PEAI/PCBM/BCP/Ag were measured outside the glove box under simulated AM 1.5G solar irradiation at 100 mW cm^{-2}. The data shown here were collected from 4 ~ 6 devices (8 ~ 12 points). For each device, the *J-V* curve was only scanned once, consisting of the forward scan (FS, – 0.2 to 1.2 V) and reverse scan (RS, 1.2 to – 0.2 V).

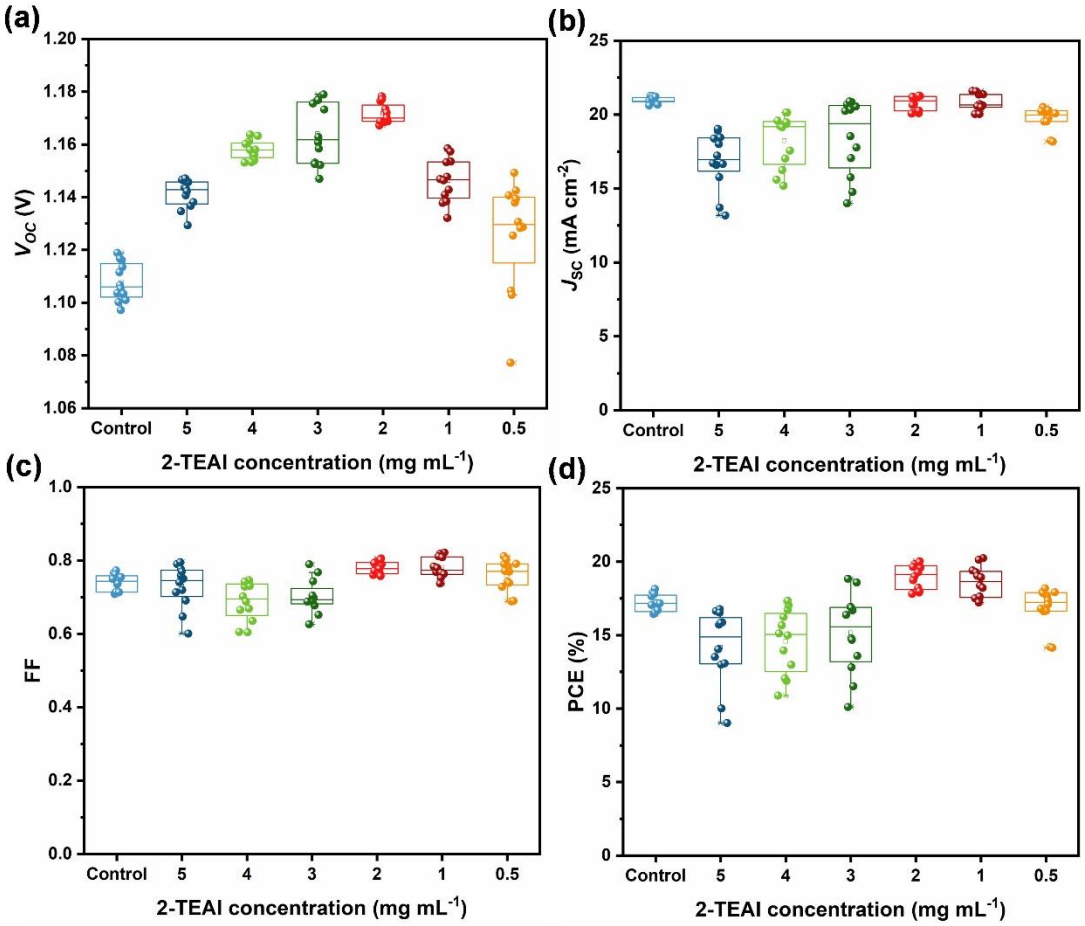

Figure S4. Statistical distributions of photovoltaic parameters (V_{OC}, J_{SC}, FF and PCE) based on the different concentrations of 2-TEAI. The devices with the structure of glass/ITO/poly-TPD/PFN-Br/perovskite/2-TEAI/PCBM/BCP/Ag were measured outside the glove box under simulated AM 1.5G solar irradiation at 100 mW cm^{-2}. The data shown here were collected from 6 devices (12 points). For each device, the *J-V* curve was only scanned once, consisting of the forward scan (FS, – 0.2 to 1.2 V) and reverse scan (RS, 1.2 to – 0.2 V).

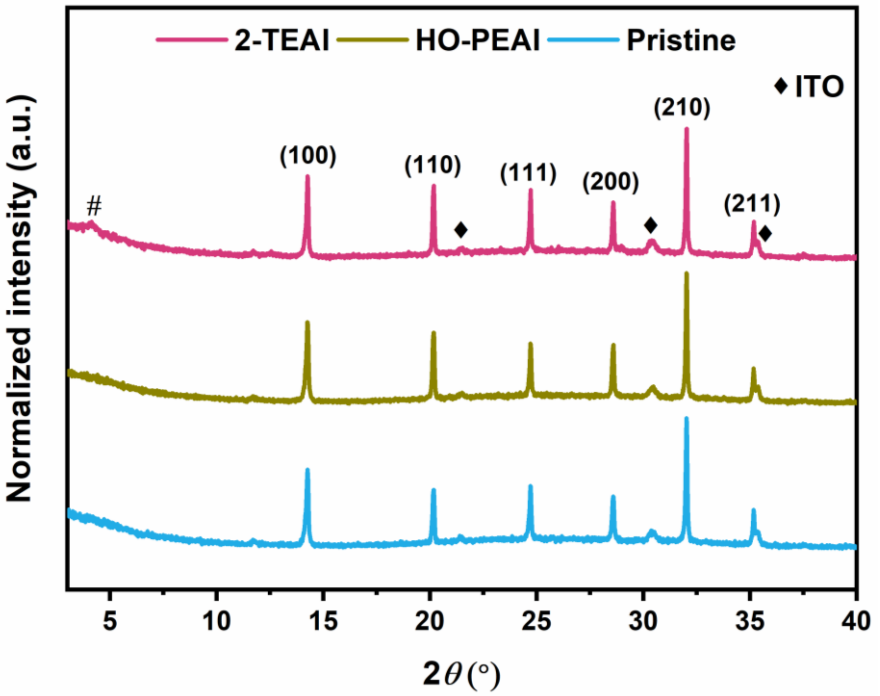

Figure S5. XRD patterns of perovskite films without and with surface modulators. Note that all these perovskite films were deposited on glass/ITO/poly-TPD. # denotes a formation of a new phase.

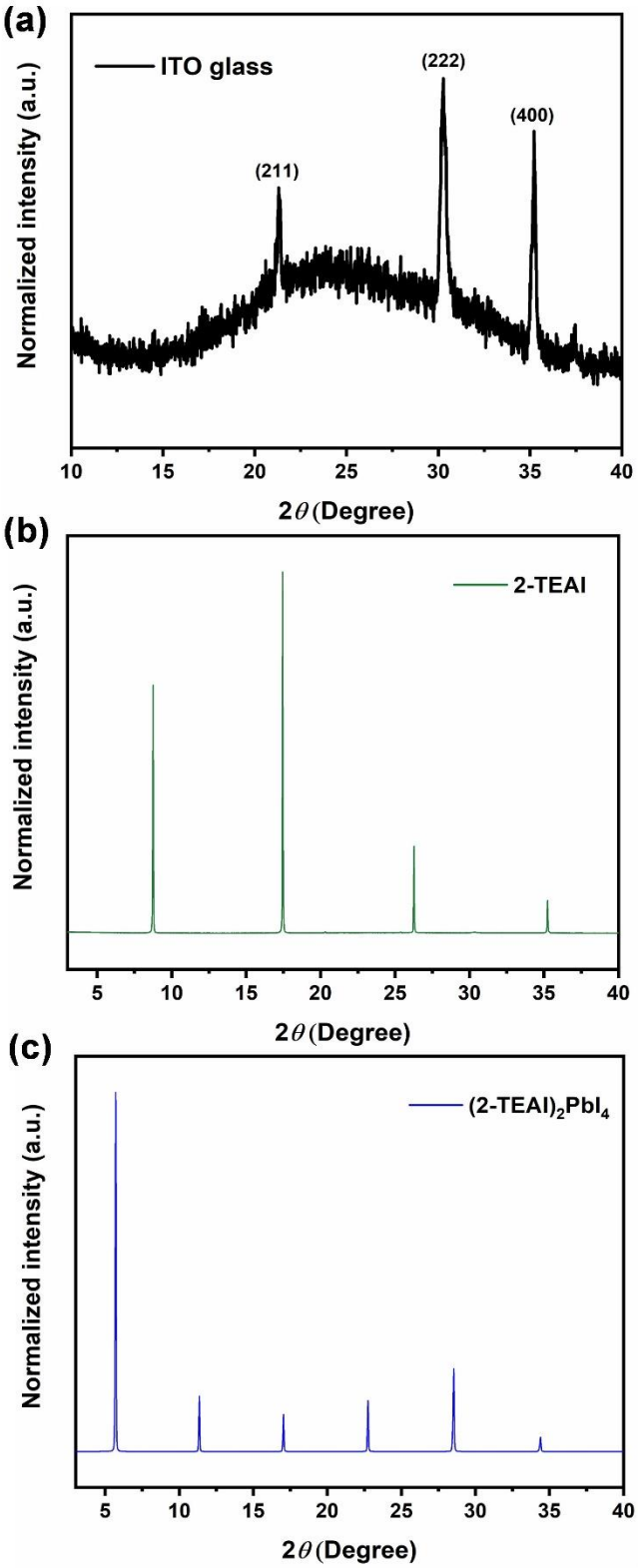

Figure S6. XRD patterns of a) ITO glass. b) 2-TEAI thin film. The 2-TEAI film is prepared by spin-coating 100 mg mL^{-1} 2-TEAI (dissolved in IPA) with a ramp of 2000 rpm (2000 rpm s^{-1}) and a time of 30 s. c) $(2\text{-TEAI})_2PbI_4$ thin film deposited on ITO glass. The $(2\text{-TEAI})_2PbI_4$ film is prepared by spin-coating 0.8 M 2-TEAI and 0.4 M PbI_2 in DMF:DMSO (4:1 V/V) on ITO glass with a ramp of 2000 rpm (2000 rpm s^{-1}) and a time of 30 s.

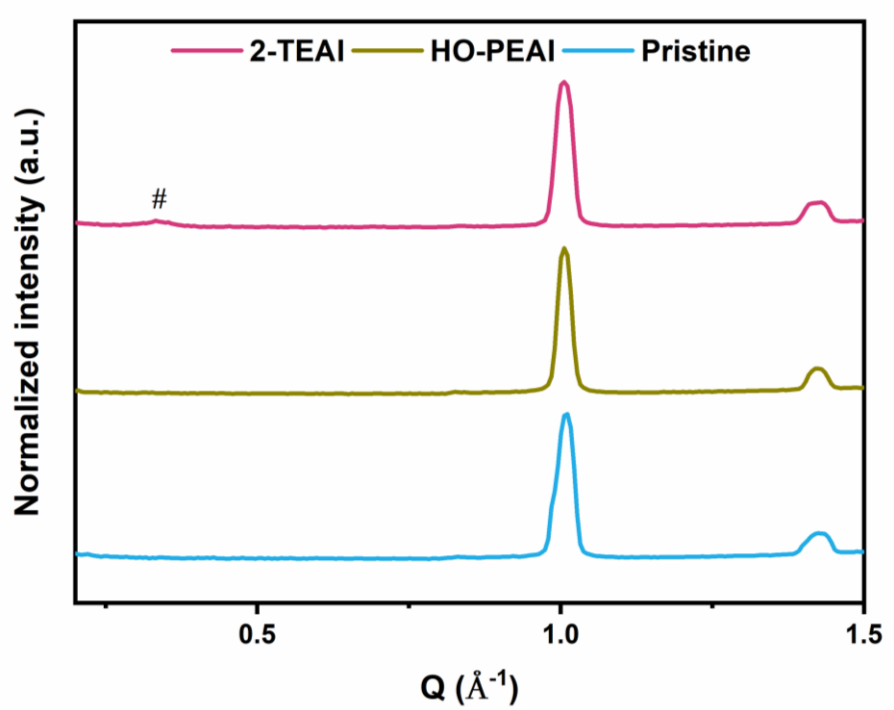

Figure S7. Azimuthally integrated 1D GIWAXS intensity profiles from the data shown in 2D maps. Note that all perovskite films were deposited on glass/ITO/poly-TPD. # denotes a formation of a new phase.

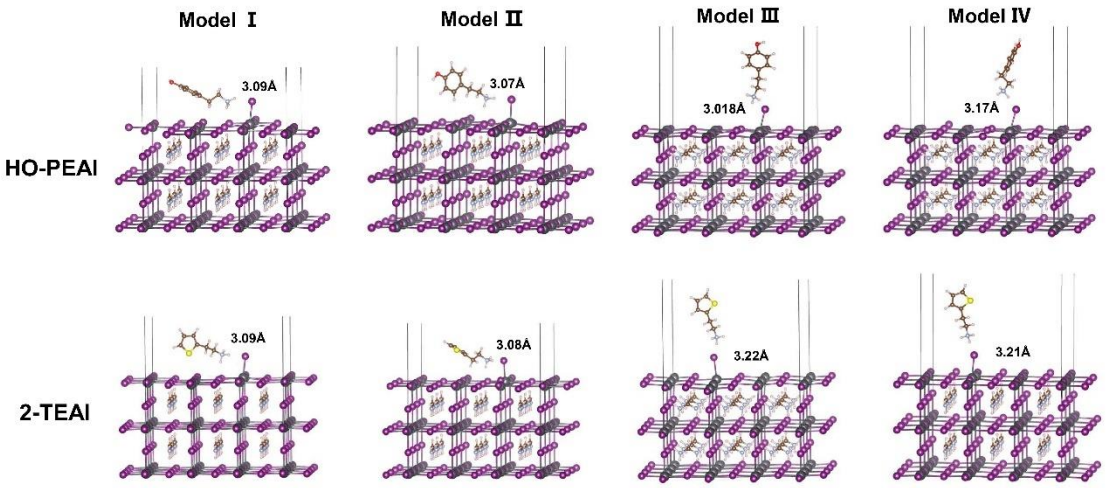

Figure S8. The optimized configurations for HO-PEAI and 2-TEAI adsorption on the PbI_2-terminated surface of $FAPbI_3$ through I-Pb bond

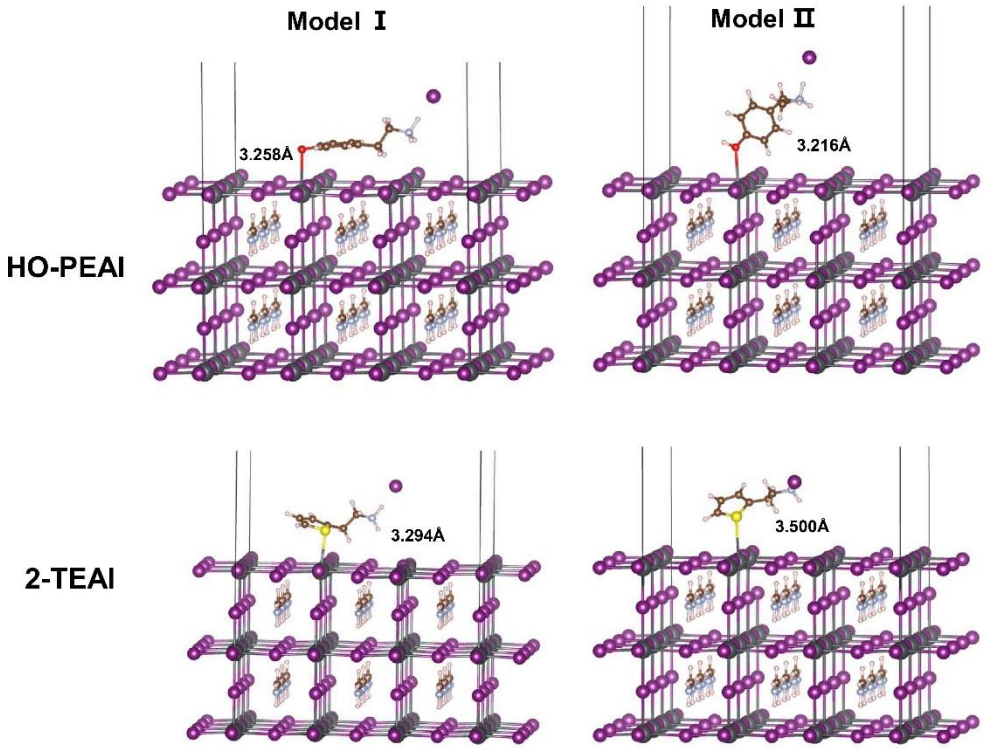

Figure S9. The optimized configurations for HO-PEAI and 2-TEAI adsorption on the PbI_2-terminated surface of $FAPbI_3$ through O-Pb or S-Pb bond, respectively.

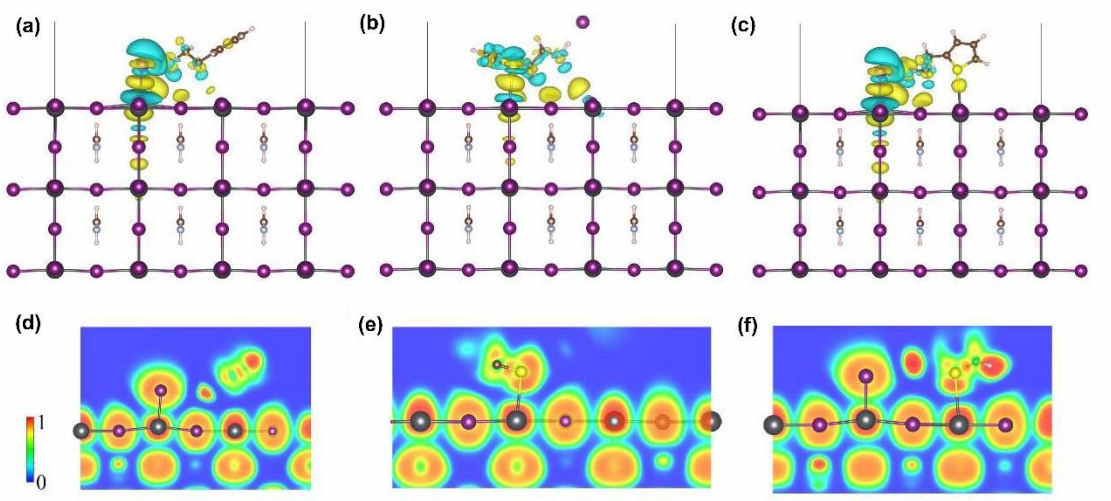

Figure S10. The charge density difference for the adsorption of 2-TEAI on the PbI_2-terminated surface of $FAPbI_3$ through a) I-Pb, b) S-Pb, and c) both I-Pb and S-Pb bond. d-f) Corresponding electron localization function (ELF).

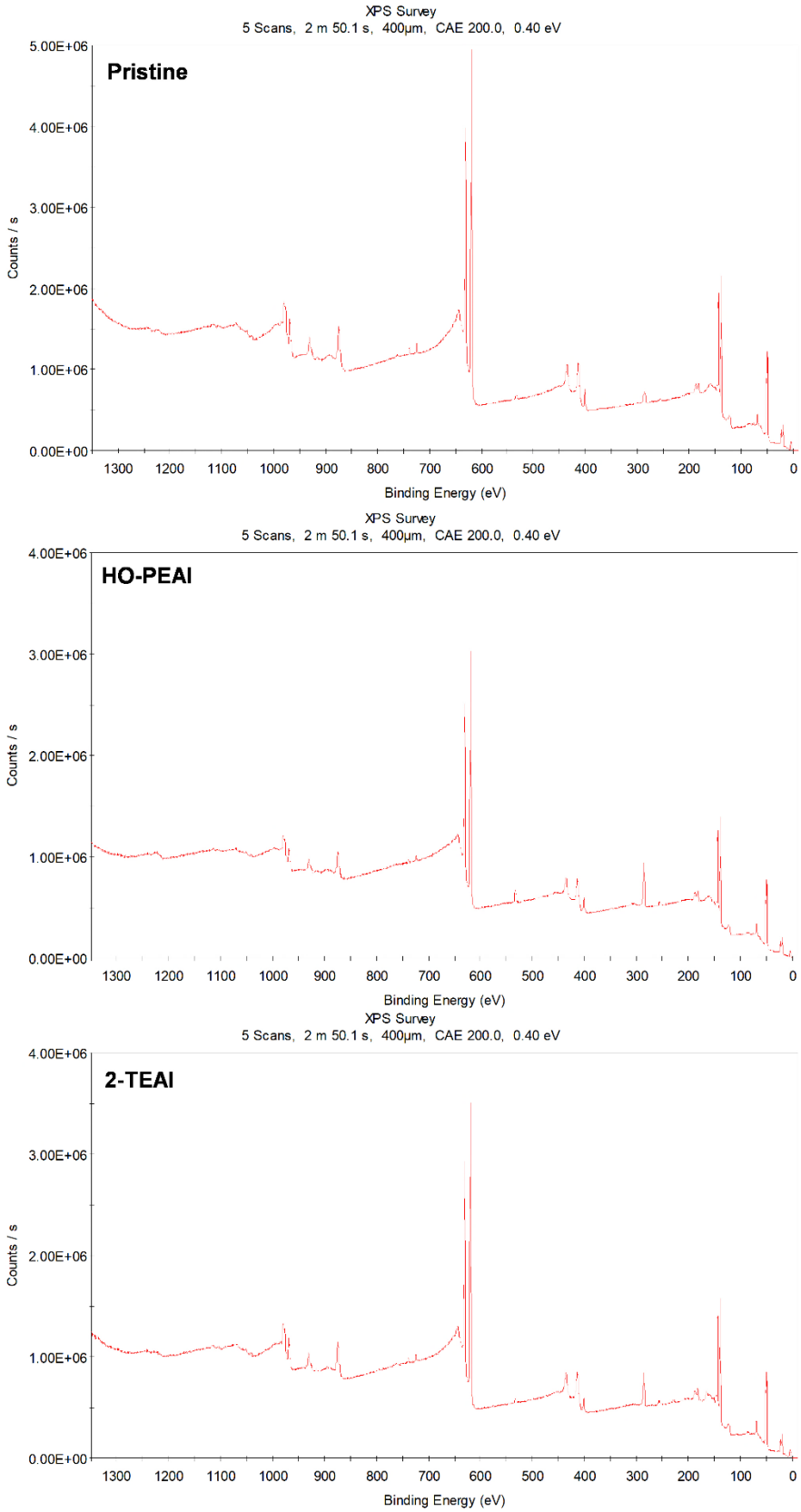

Figure S11. XPS survey spectra of perovskite films without and with surface modulators. Note that all these perovskite films were deposited on glass/ITO/poly-TPD.

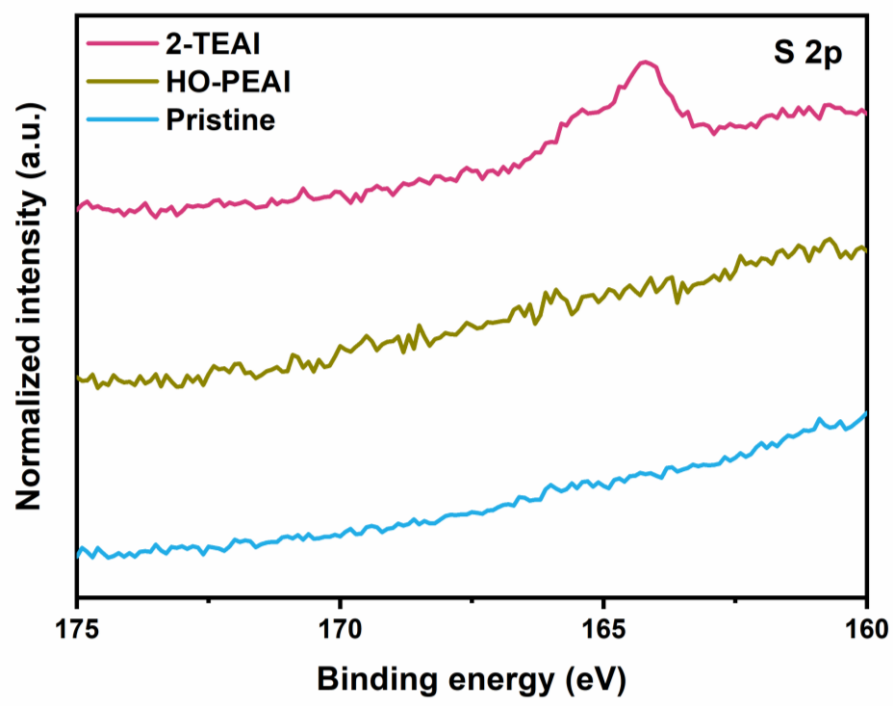

Figure S12. S 2p core-level spectra of perovskite films without and with surface modulators. Note that all these perovskite films were deposited on glass/ITO/poly-TPD.

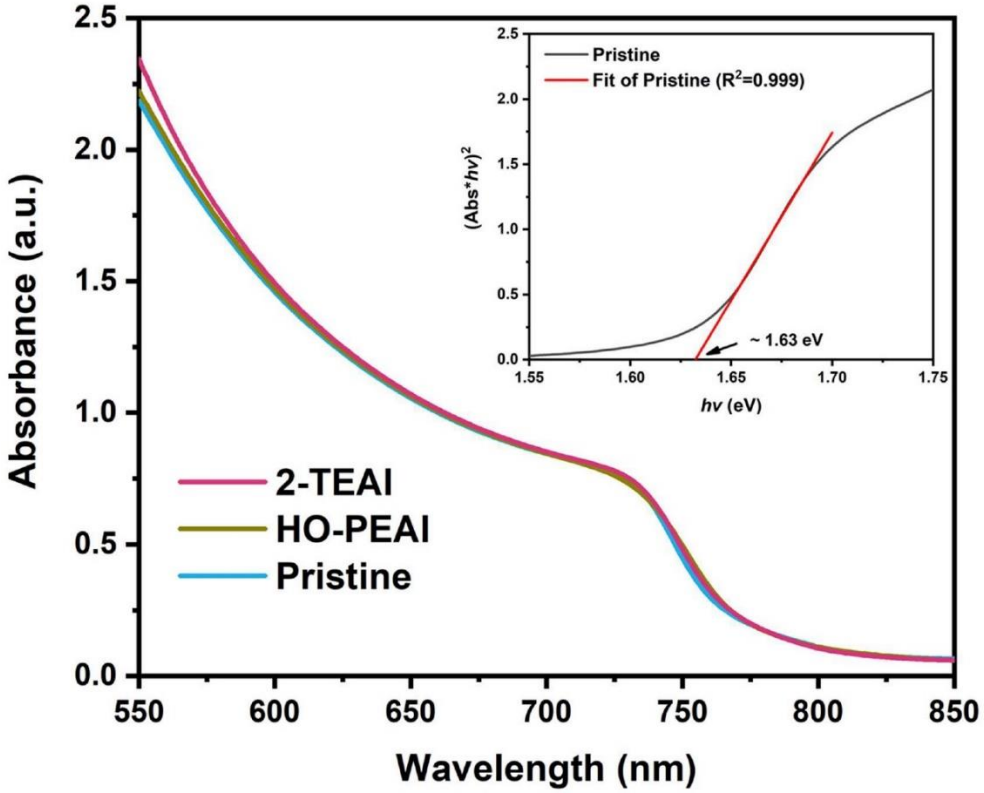

Figure S13. UV-Vis spectrum of different perovskite films. Note that all these perovskite films were deposited on glass/ITO/poly-TPD. The inset figure is the optical bandgap obtained from the Tauc plot.

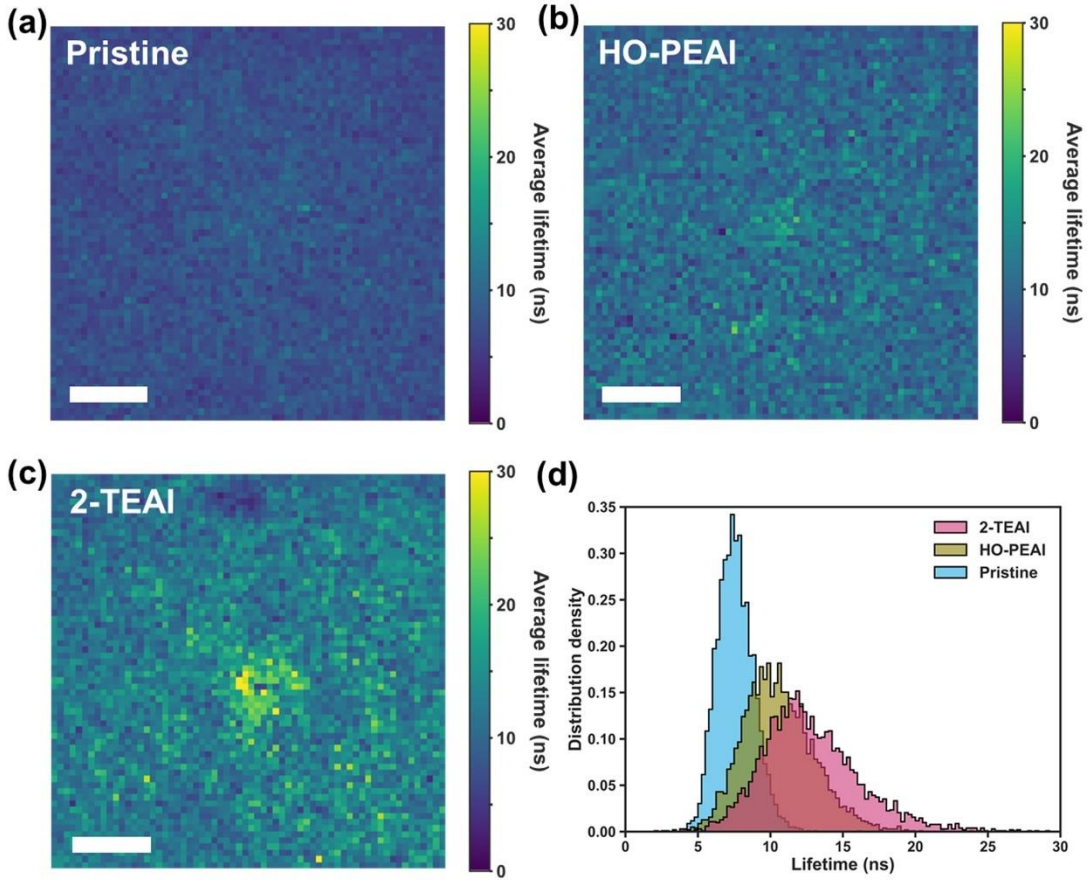

Figure S14. a-c) The carrier lifetime maps of perovskite films without and with surface treatments. The scalebar is 20 μm. d) Distribution of the carrier lifetime obtained from the maps. Note that all these perovskite films were deposited on glass/ITO/poly-TPD. The sample was excited by a 405 nm pulsed diode with 1 $\mu J/cm^2$/pulse fluence.

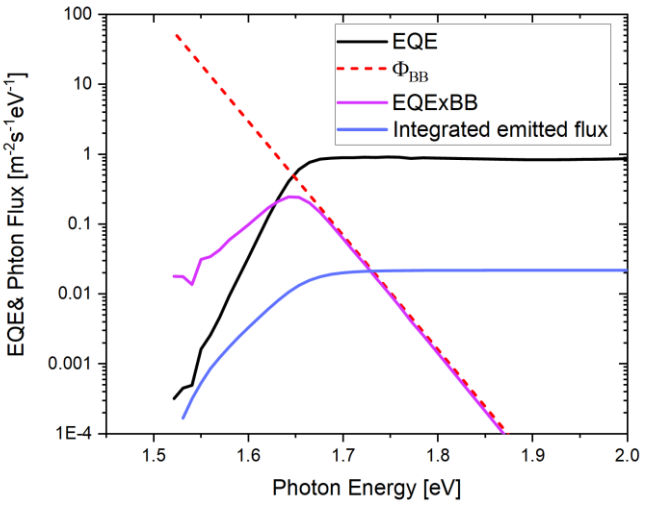

Figure S15. EQE_{PV} onset (black line) convoluted with the black-body (ϕ_{BB}) radiation of the surroundings at 300K (red dotted line). The perovskite emission spectrum from the convolution is plotted in purple. The latter emission spectra are integrated over the photon energy and multiplied by the elementary charge q to calculate the dark radiative current $J_{0,\,rad}$, plotted in blue.

The approach follows the report by Rau et al.[11] Briefly the black body photon flux is

$$\phi_{BB} = \frac{1}{4\pi^2\hbar^3c^2}\frac{E^2}{\exp\left(\frac{E}{k_BT}\right)-1} \tag{S2}$$

with ħ Planck's constant, k_B Boltzmann constant and T temperature. Assuming that the perovskite solar cell is at 300K in thermal equilibrium with its environment, the dark radiative recombination current is:

$$J_{em,0} = q\int EQE_{PV}(E)\phi_{BB}(E)dE = J_{rad,0} \tag{S3}$$

with EQE_{PV} the photovoltaic *external* quantum efficiency of the perovskite solar cell and $J_{em,0}$ the current giving rise to emission, which also defines the dark radiative recombination current at $V = 0$. In our case, we find $J_{rad,0} = 3.5 \cdot 10^{-21}\ A/m^2$. From that, the QFLS can be calculated with the following equation:

$$QFLS = \frac{k_BT}{q}\ln\left(\frac{J_G}{J_{rad,0}}\cdot PLQY\right) \tag{S4}$$

where J_G is the generation current under illumination, in this case approximated to the short circuit current J_{sc}.

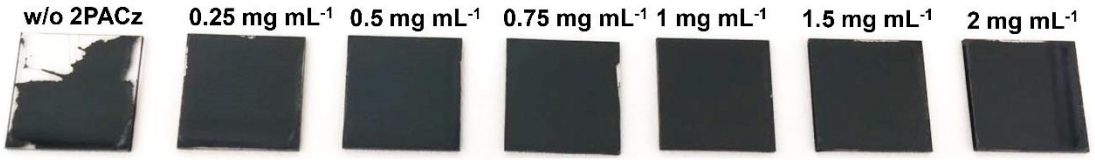

Figure S16. Photos of the perovskite films based on the different concentrations of 2PACz. The structure is glass/ITO/poly-TPD/2PACz/perovskite. For all samples, the perovskite solution was intentionally spread on the substrate by pipette tips before spin-coating.

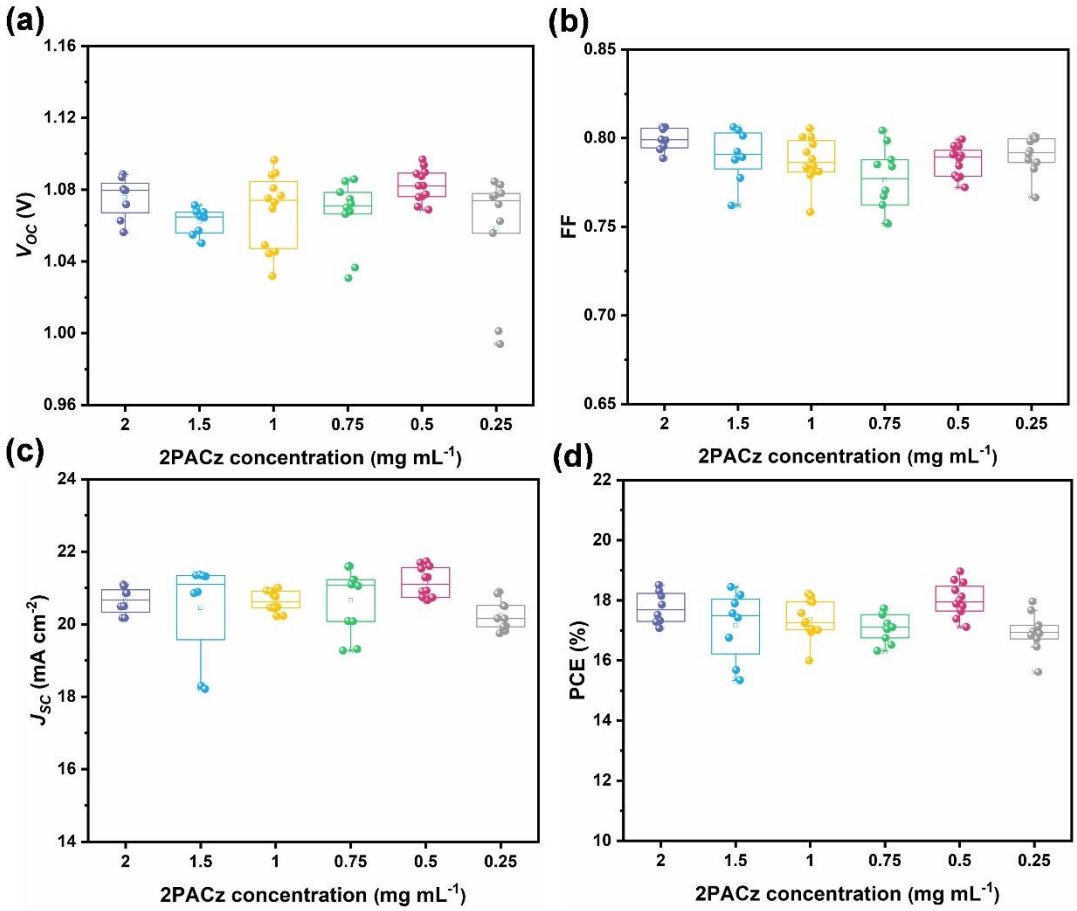

Figure S17. Statistical distributions of photovoltaic parameters (V_{OC}, FF, J_{SC} and PCE) based on the different concentrations of 2PACz. The devices with the structure of glass/ITO/poly-TPD/2PACz/perovskite/PCBM/BCP/Ag were measured outside the glove box under simulated AM 1.5G solar irradiation at 100 mW cm^{-2}. The data shown here are collected from 4 ~ 6 devices (8 ~ 12 points). For each device, the J-V curve was only scanned once, consisting of the forward scan (FS, – 0.2 to 1.2 V) and reverse scan (RS, 1.2 to – 0.2 V). Here we found that the 2PACz did not improve the device performance compared to our previous studies of fluorene-based conjugated polyelectrolytes (CPEs),[3,12] but it provides a new strategy to overcome the de-wetting issue of hydrophobic poly-TPD.

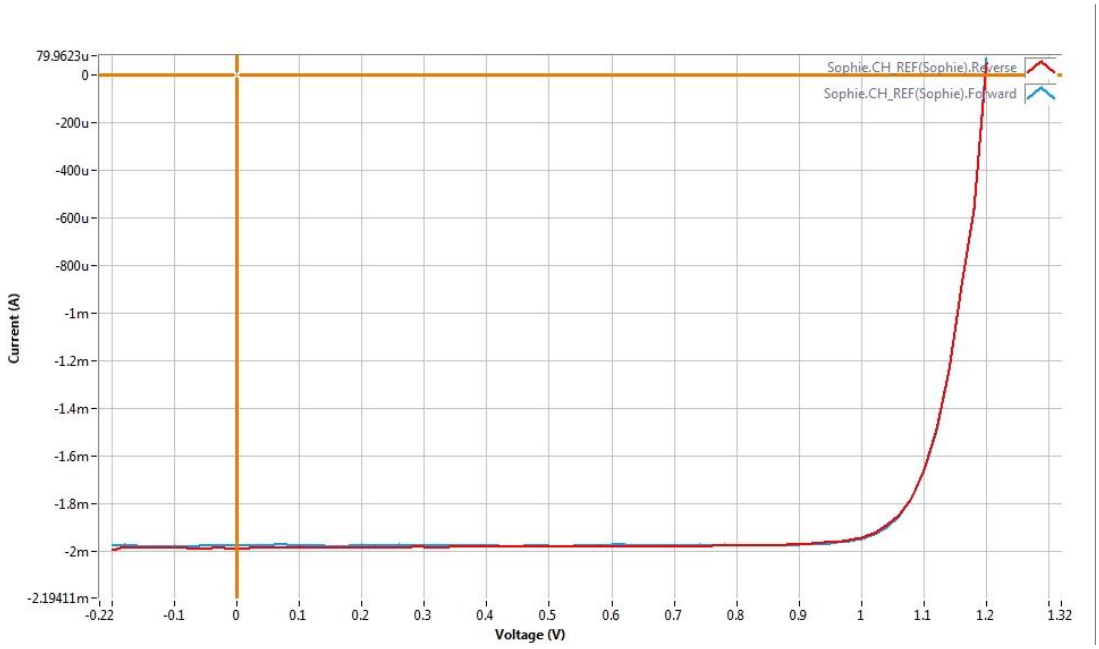

Figure S18. Original *I-V* curves of the champion device based on the 2-TEAI treatment. The figure was captured by IVS-KA5000 software (Enlitech) during the measurement and the device was only scanned once. The device has a structure of glass/ITO/poly-TPD/2PACz/perovskite/2-TEAI/PCBM/BCP/Ag. The devices were measured outside the glove box under simulated AM 1.5G solar irradiation at 100 mW cm^{-2}. The *I-V* curves are composed of the forward scan (FS, – 0.2 to 1.2 V) and reverse scan (RS, 1.2 to – 0.2 V). The aperture area of the mask is 0.09 cm^2 (the active area is ~ 0.25 cm^2) for calculating the current densities in *J-V* curves.

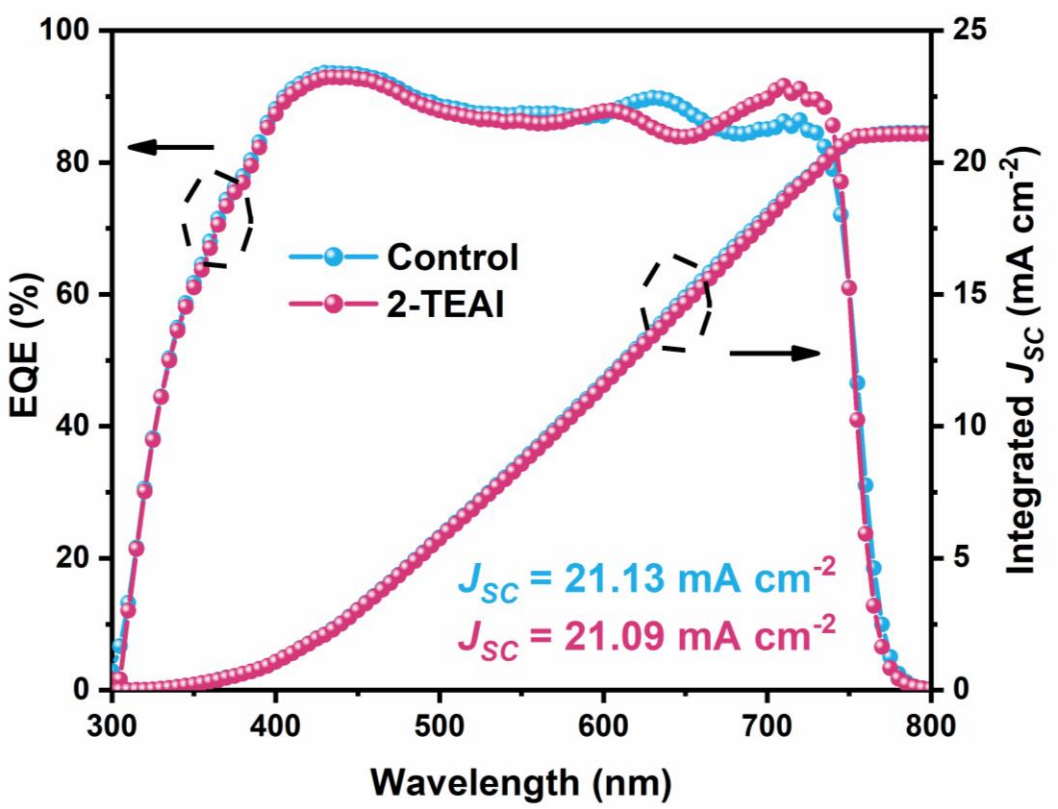

Figure S19. EQE spectrum for the champion cell of control and 2-TEAI devices.

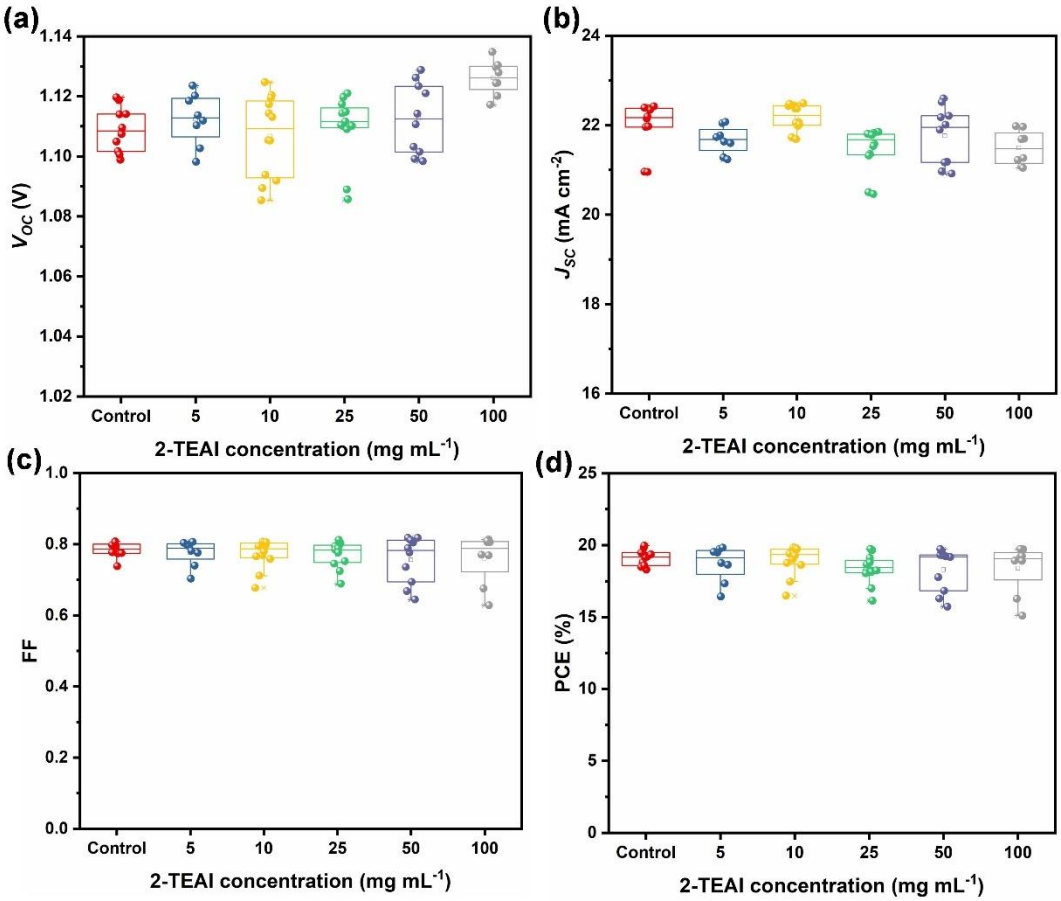

Figure S20. Statistical distributions of photovoltaic parameters (V_{OC}, J_{SC}, FF and PCE) based on the different concentrations of 2-TEAI at the perovskite bottom. The devices with the structure of glass/ITO/poly-TPD/2PACz/2-TEAI/perovskite/PCBM/BCP/Ag were measured outside the glove box under simulated AM 1.5G solar irradiation at 100 mW cm^{-2}. The data shown here were collected from 4 ~ 6 devices (8 ~ 12 points). For each device, the *J-V* curve was only scanned once, consisting of the forward scan (FS, – 0.2 to 1.2 V) and reverse scan (RS, 1.2 to – 0.2 V).

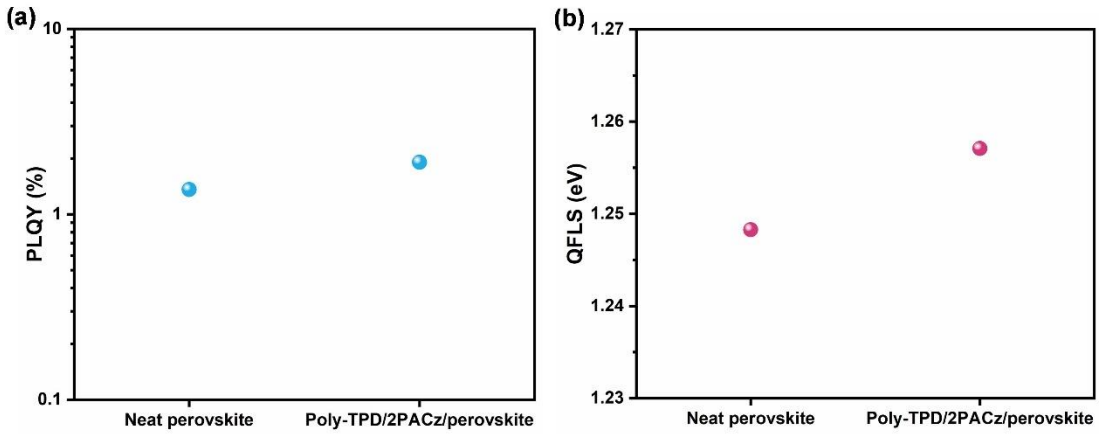

Figure S21. PLQY and calculated QFLS of perovskite deposited on bare glass and poly-TPD coated ITO glass. Note that the neat perovskite has a structure of glass/perovskite while the other has a structure of glass/ITO/poly-TPD/2PACz/perovskite.

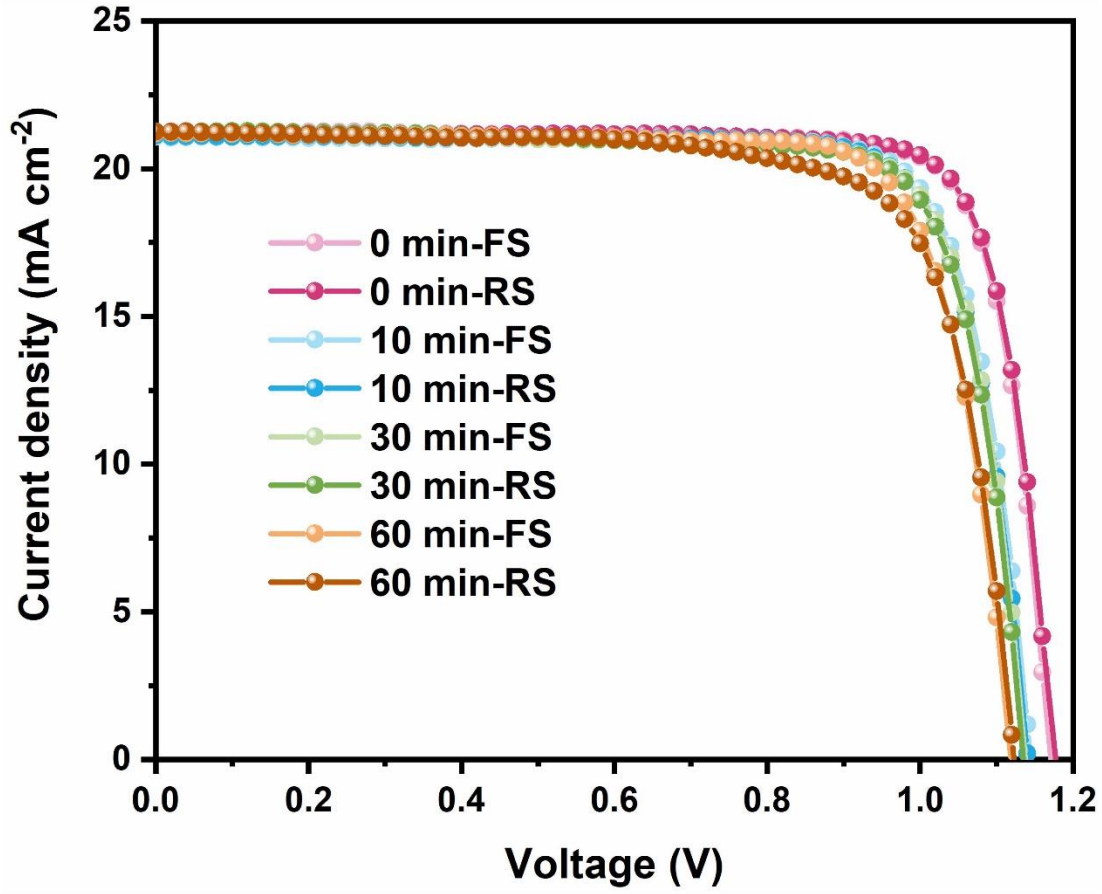

Figure S22. *J-V* curves vary with the annealing time of 2-TEAI. The devices with a structure of glass/ITO/poly-TPD/2PACz/perovskite/2-TEAI/PCBM/BCP/Ag were measured outside the glove box under simulated AM 1.5G solar irradiation at 100 mW cm^{-2}. For each scan, the *J-V* curves are composed of the forward scan (FS, – 0.2 to 1.2 V) and reverse scan (RS, 1.2 to – 0.2 V) and both were only scanned one time. Note that the annealing time was recorded after spin-coating 2-TEAI on as-crystalized perovskite film.

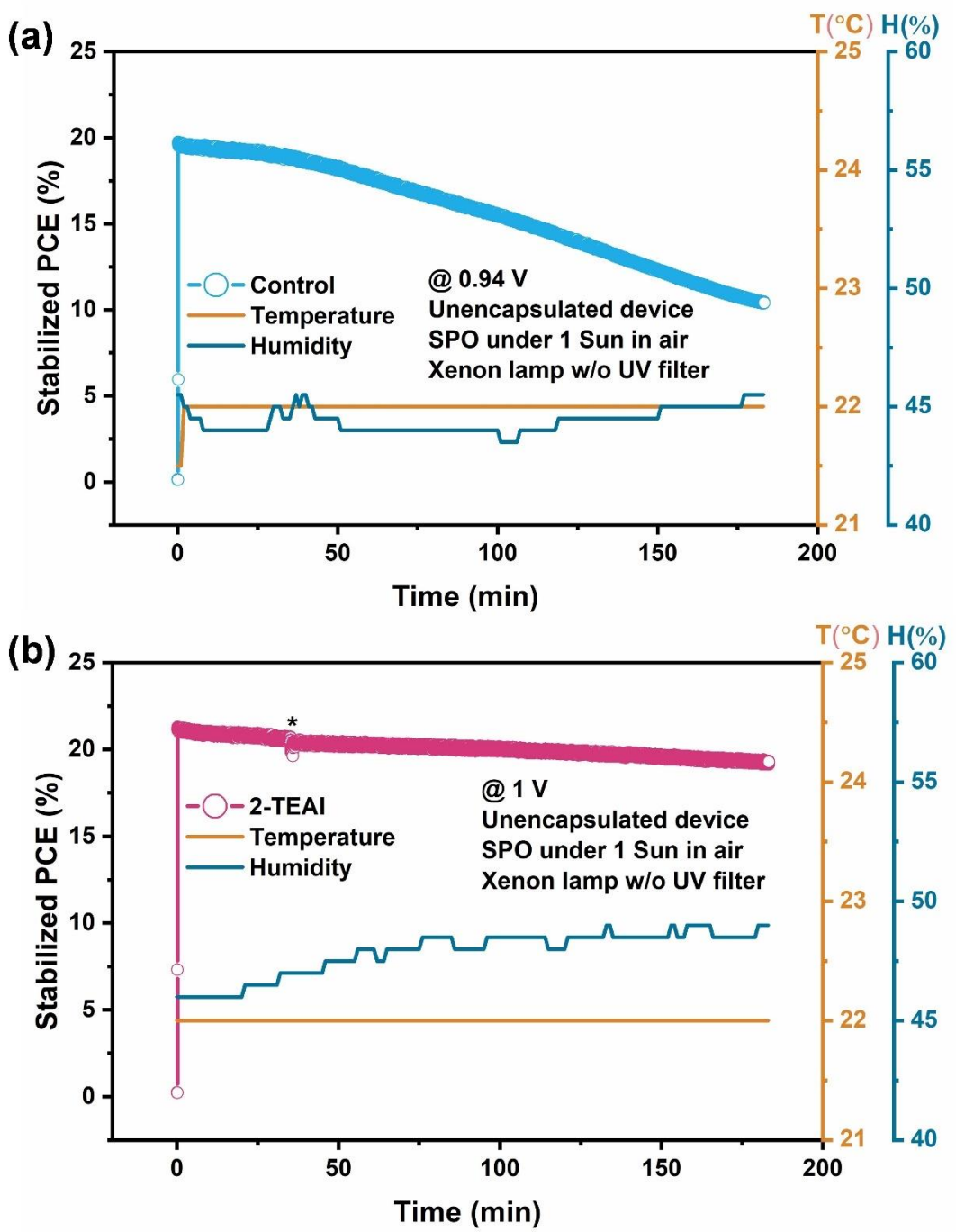

Figure S23. Comparison of stabilized power output (SPO) under continuous illumination at the V_{MPP}. a) Control device measured at a V_{MPP} of 0.94 V with a structure of glass/ITO/poly-TPD/2PACz/perovskite/PCBM/BCP/Ag. b) 2-TEAI-passivated device measured at a V_{MPP} of 1 V with a structure of glass/ITO/poly-TPD/2PACz/perovskite/2-TEAI/PCBM/BCP/Ag. Note that a small fluctuation (denoted with *) is caused by a small disturbance of the measurement. The illumination source is identical to the *J-V* measurements based on a AAA steady solar simulator under AM 1.5G (100 mW cm^{-2}). The PCE data were collected every 1 s. The room temperature and relative humidity were recorded every 60 s. For device surface, the actual temperature is much higher due to the heating effects of the illumination.

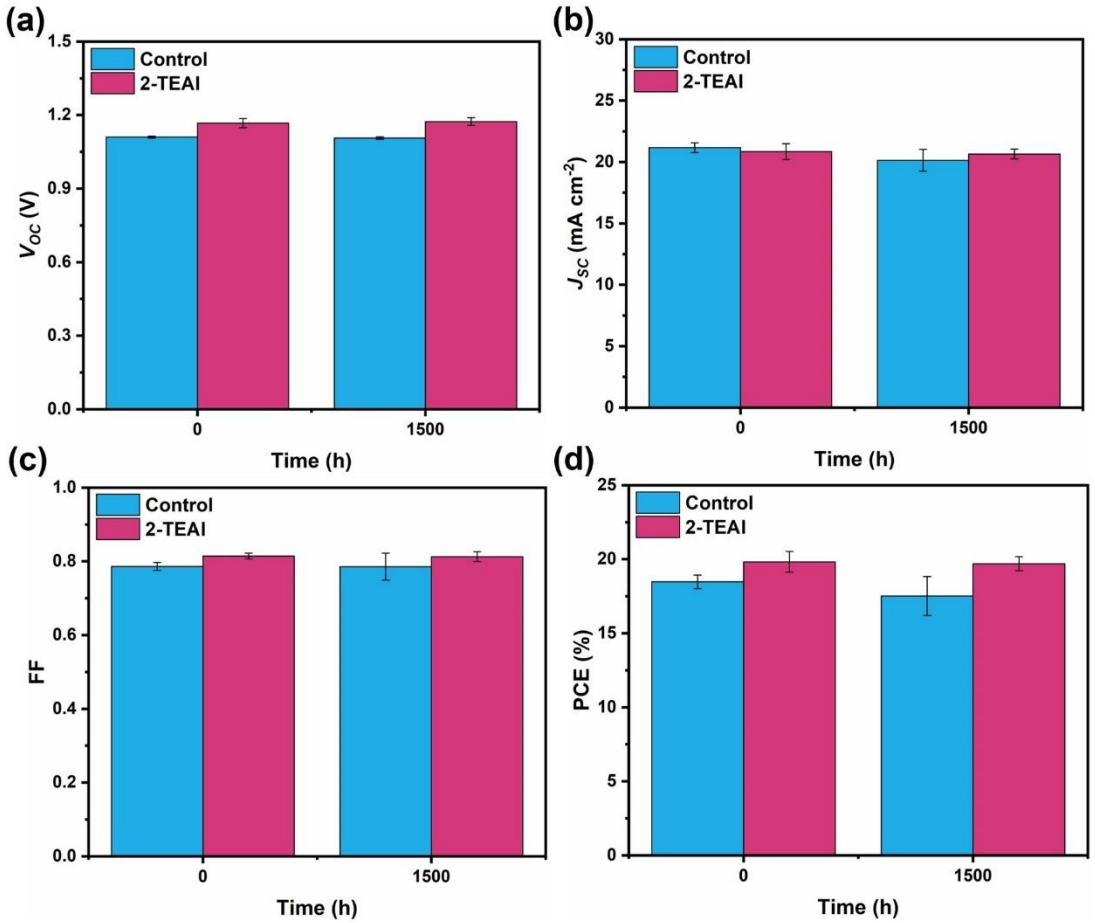

Figure S24. Device performance at dark storage in N_2-filled glove box for 1500 h. The control devices with a structure of glass/ITO/poly-TPD/2PACz/perovskite/PCBM/BCP/Ag and the 2-TEAI devices with a structure of glass/ITO/poly-TPD/2PACz/perovskite/2-TEAI/PCBM/BCP/Ag were measured outside the glove box under simulated AM 1.5G solar irradiation at 100 mW cm^{-2}. The data were obtained from five control devices and six 2-TEAI devices, in which the devices were randomly selected for the measurement. For each device, the data shown here were the average values of forward scan (FS, – 0.2 to 1.2 V) and reverse scan (RS, 1.2 to – 0.2 V) and both were only scanned once for each time.

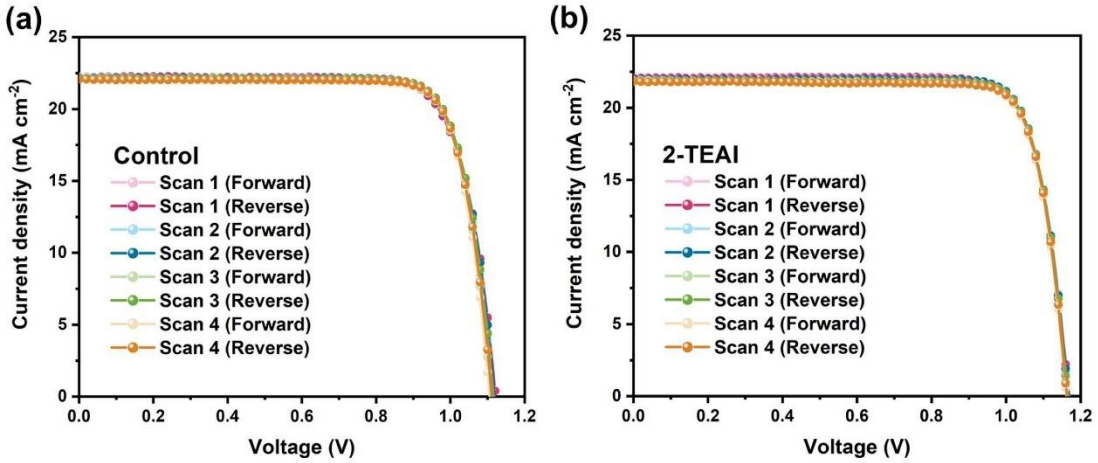

Figure S25. *J-V* curves of control or 2-TEAI device based on the different scans. The control device has the structure of glass/ITO/poly-TPD/2PACz/perovskite/PCBM/BCP/Ag whilst the 2-TEAI device has the structure of glass/ITO/poly-TPD/2PACz/perovskite/2-TEAI/PCBM/BCP/Ag. The devices were measured outside the glove box under simulated AM 1.5G solar irradiation at 100 mW cm^{-2}. For each scan, the *J-V* curves are composed of the forward scan (FS, – 0.2 to 1.2 V) and reverse scan (RS, 1.2 to – 0.2 V). During this measurement, the devices were fixed under a solar simulator and the second scan started immediately after the first scan. Before the first scan, there is no pre-light or pre-bias treatment for the devices and the shutter is automatically closed between each scan. The results indicate that the devices are light soaking free. Therefore, all the devices are only scanned once for the *J-V* measurements in our study.

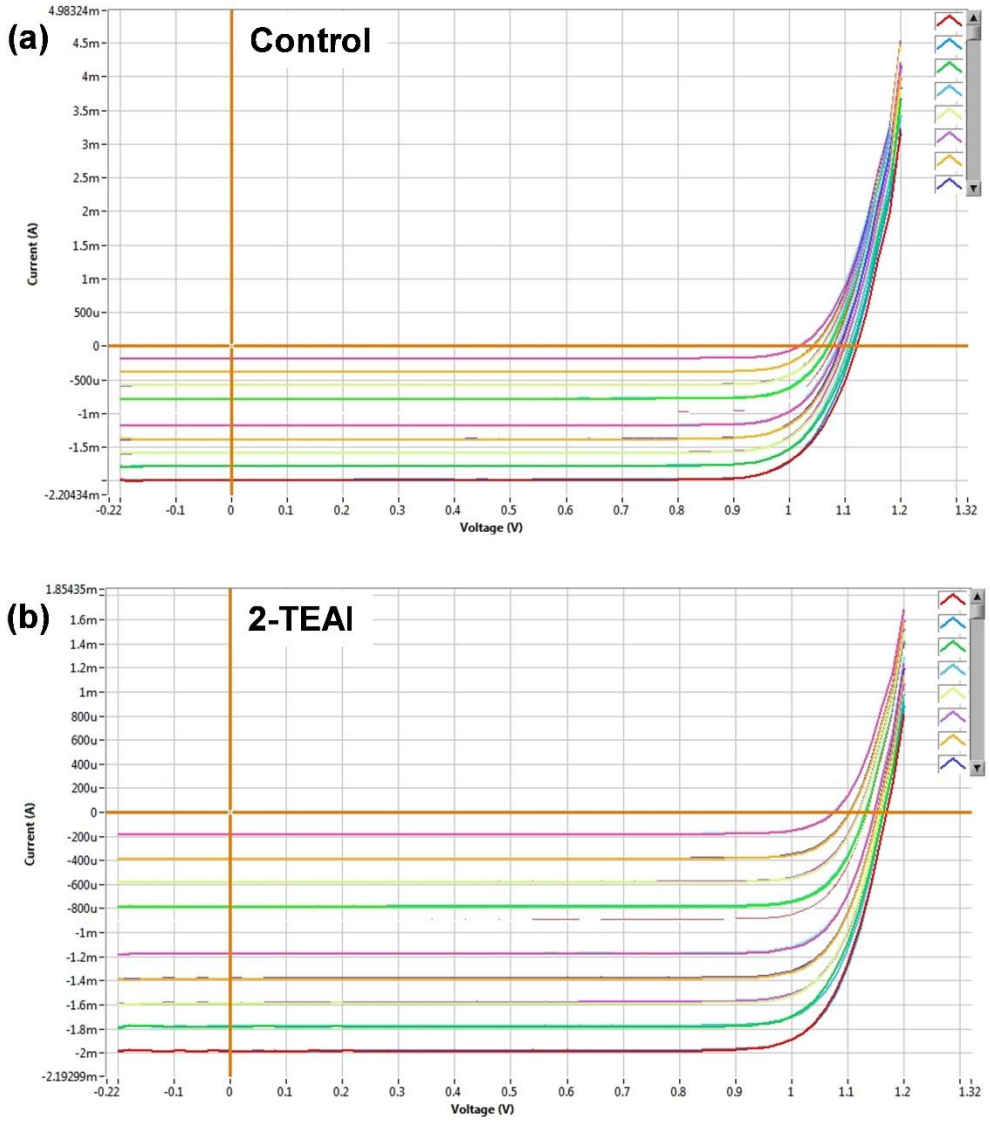

Figure S26. Original *I-V* curves of control or 2-TEAI device based on the different light intensities. The figure was captured by IVS-KA5000 software (Enlitech) during the measurement and the device was only scanned once at each intensity. Note that the *J*-V curves shown here were composed of the forward scan (FS, – 0.2 to 1.2 V) and reverse scan (RS, 1.2 to – 0.2 V). For this measurement, the control was used the champion device (with an average V_{OC} of 1.12 V, J_{SC} of 22.12 mA cm^{-2}, FF of 0.81 and PCE of 20% obtained from reverse and forward scan) while the 2-TEAI device was randomly selected (with an average V_{OC} of 1.17 V, J_{SC} of 22.07 mA cm^{-2}, FF of 0.82 and PCE of 21% obtained from reverse and forward scan).

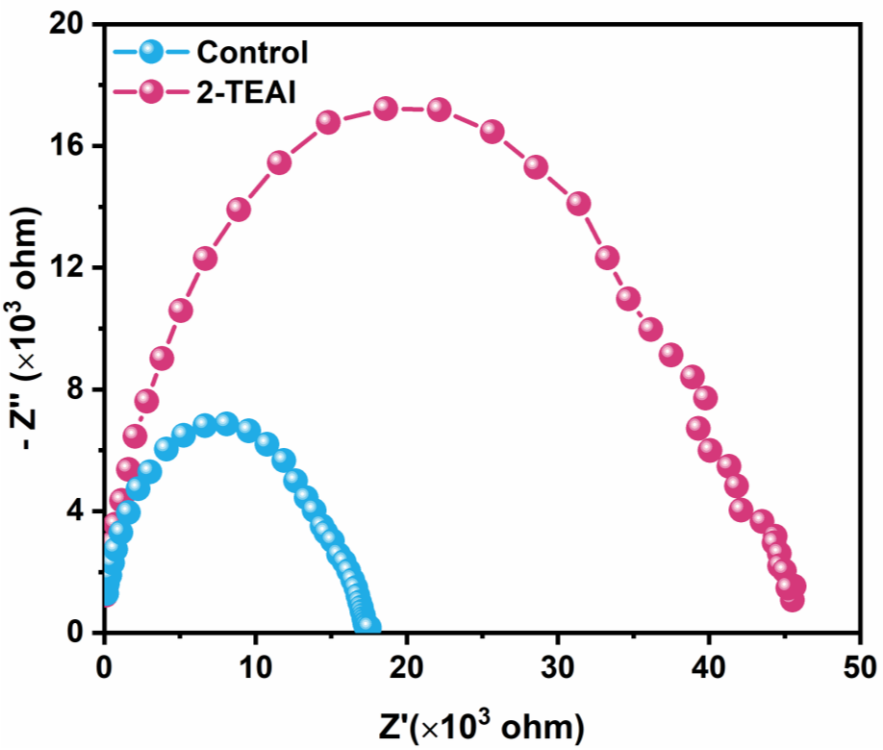

Figure 27. Nyquist plots of the EIS measurements for control and 2-TEAI devices.

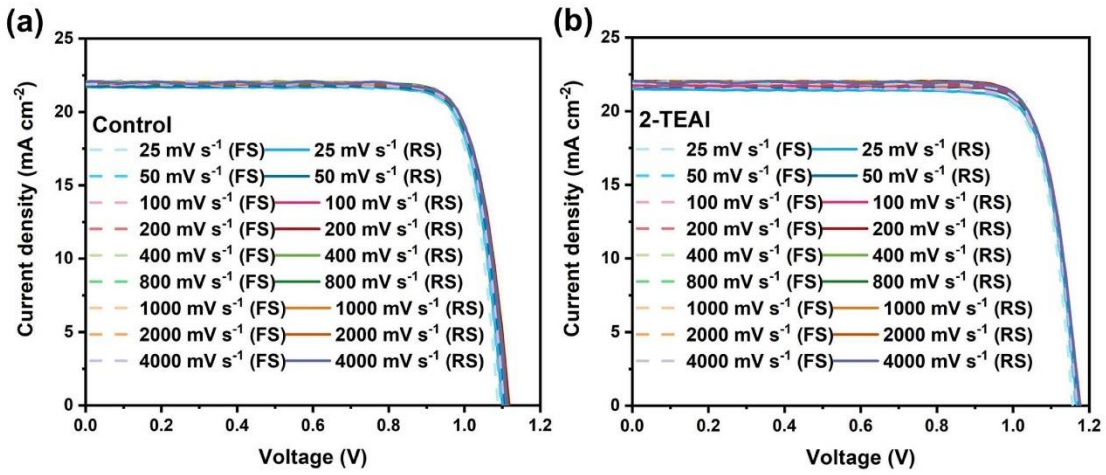

Figure S28. *J-V* curves of control or 2-TEAI device based on the different scan rates. The control device has the structure of glass/ITO/poly-TPD/2PACz/perovskite/PCBM/BCP/Ag whilst the 2-TEAI device has the structure of glass/ITO/poly-TPD/2PACz/perovskite/2-TEAI/PCBM/BCP/Ag. The devices were measured outside the glove box under simulated AM 1.5G solar irradiation at 100 mW cm^{-2}. For each scan, the *J-V* curves are composed of the forward scan (FS, – 0.2 to 1.2 V) and reverse scan (RS, 1.2 to – 0.2 V) and both were only scanned once for each time.

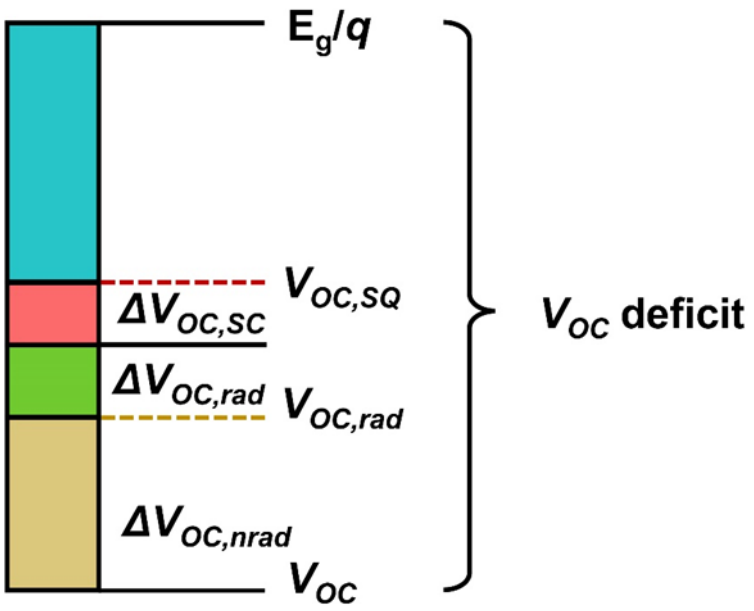

Figure S29. Schematic of V_{OC} deficit in PSCs. The detailed components of V_{OC} deficit (defined as $E_g/q - V_{OC}$, E_g is the optical band gap and q is an electric charge) include $V_{OC,\,SQ}$ (Shockley-Queisser, SQ limit of V_{OC}) and $V_{OC,\,rad}$ (radiative limit of V_{OC}).

For most PSCs, the ($E_g/q - V_{OC,\,SQ}$) is a constant of ~ 0.28 V.[26] Hence, the V_{OC} loss is determined by the difference between $V_{OC,\,SQ}$ and V_{OC}, defined as the following equation :[27]

$$V_{OC,\,SQ} - V_{OC} = \frac{K_B T}{q}\ln\left(\frac{J_{SC,SQ}}{J_{0,SQ}}\right) - \frac{K_B T}{q}\ln\left(\frac{J_{SC}}{J_0}\right) = \frac{K_B T}{q}\ln\left(\frac{J_{SC,SQ}}{J_{SC}} \times \frac{J_{0,rad}}{J_{0,SQ}} \times \frac{J_0}{J_{0,\,rad}}\right)$$

$$= \Delta V_{OC,\,SC} + \Delta V_{OC,\,rad} + \Delta V_{OC,\,nrad} \quad \text{(S5)}$$

Where K_B is the Boltzmann constant, T is temperature, and q is the electric charge. $\Delta V_{OC,\,SC}$ is the V_{OC} loss in short-circuit current density, $\Delta V_{OC,\,rad}$ is radiative V_{OC} loss, $\Delta V_{OC,\,nrad}$ is non-radiative V_{OC} loss. According to equation (1), the V_{OC} loss is composed of three parts, namely $\Delta V_{OC,\,SC}$, $\Delta V_{OC,\,rad}$ and $\Delta V_{OC,\,nrad}$, in which the $\Delta V_{OC,\,nrad}$ is due to the non-radiative recombination. Considering only ~ 0.01 V for the sum of $\Delta V_{OC,\,SC}$ and $\Delta V_{OC,\,rad}$ (also called $\Delta V_{OC,\,abs}$) in solution-processed inverted PSCs,[28] the V_{OC} loss is fundamentally affected by the $\Delta V_{OC,\,nrad}$.

$$\Delta V_{OC,\,nrad} = -\frac{K_B T}{q}\ln\left(\frac{J_{0,rad}}{J_0}\right) = -\frac{K_B T}{q}\ln\left(\frac{EQE_{EL} \times J_0}{J_0}\right) = -\frac{K_B T}{q}\ln EQE_{EL} \quad \text{(S6)}$$

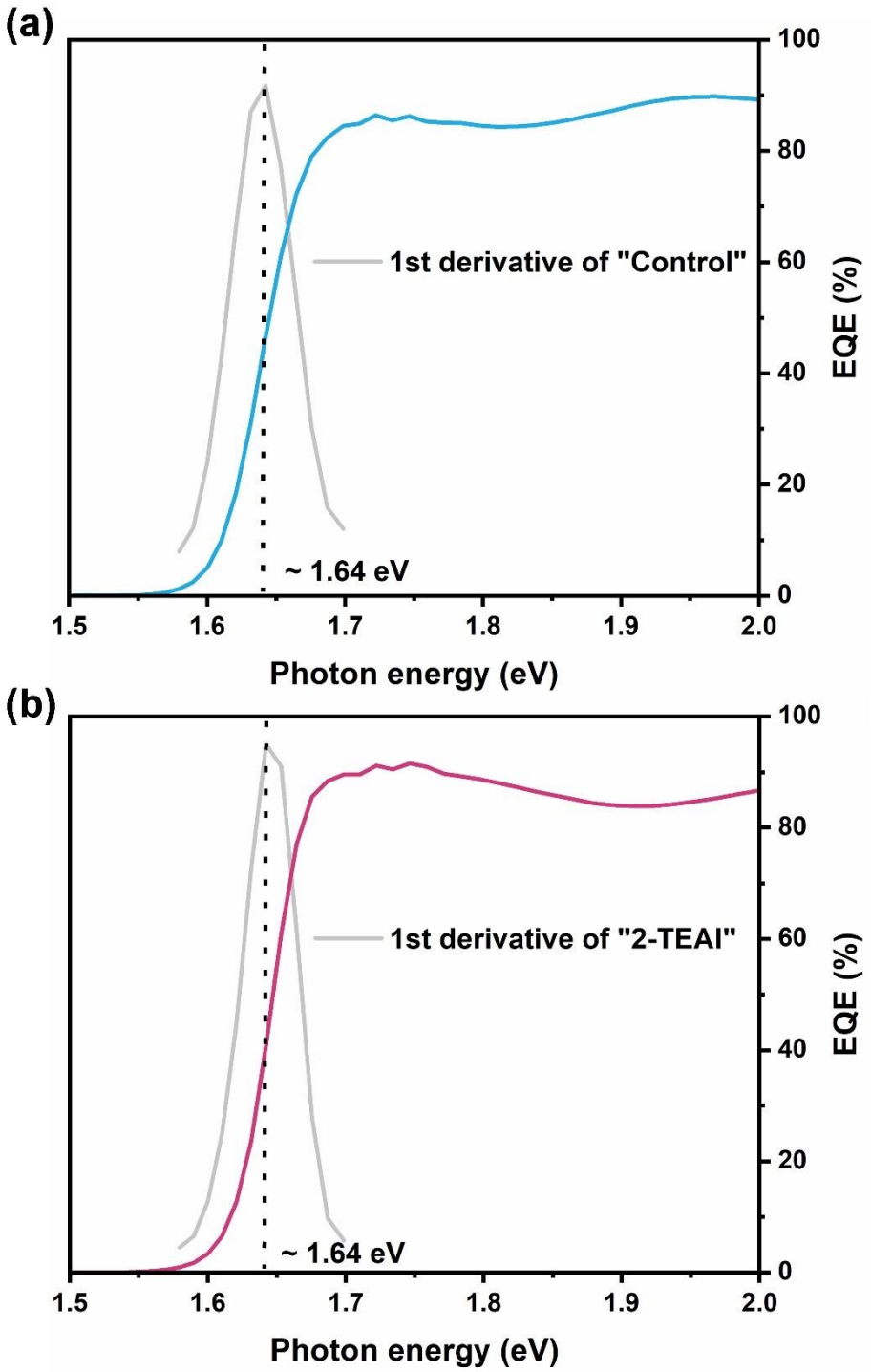

Figure 30. A band gap value of 1.64 eV is extracted from the first derivative of the EQE (grey line) as a function of photon energy for a) control and b) 2-TEAI device.

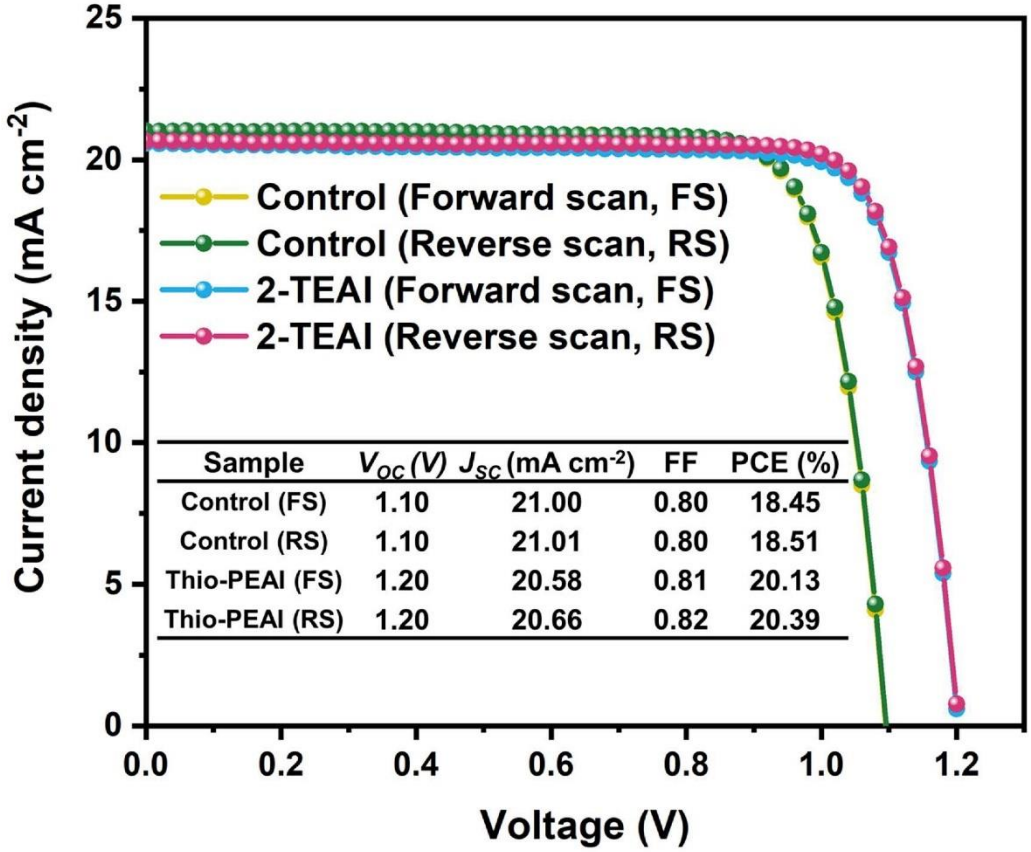

Figure S31. *J-V* curves of devices for TPV and EL measurements. Note that the devices were randomly selected and both were only scanned once for the *J-V* curves, consisting of the forward scan (FS, – 0.2 to 1.2 V) and reverse scan (RS, 1.2 to – 0.2 V).

	HOMO (eV)	**LUMO (eV)**	**Debye (D)**
HO-PEA$^+$	– 9.732	– 5.511	15.13
2-TEA$^+$	– 9.266	– 5.403	13.11

Table S1. DFT data of HO-PEA$^+$ and 2-TEA$^+$, consisting of energy level and dipole moment.

Table S2. Adsorption energy (ΔE_{ads}) of HO-PEAI and 2-TEAI on the PbI_2-terminated surface of $FAPbI_3$ through I-Pb bond.

	Model I	Model II	Model III	Model IV
HO-PEAI	– 0.9852	– 1.1560	– 0.7800	– 0.7710
2-TEAI	– 1.1099	– 1.2396	– 0.7102	– 0.7518

Table S3. Adsorption energy (ΔE_{ads}) of HO-PEAI and 2-TEAI on the PbI_2-terminated surface of $FAPbI_3$ through O-Pb and S-Pb bond, respectively.

	Model I	Model II
HO-PEAI	– 0.2772	– 0.2520
2-TEAI	– 0.4433	– 0.3380

Table S4. Surface electronic data obtained from UPS measurements. For each sample, 4-5 different areas were scanned (the rows in the table) to confirm the consistency. The average values were used to plot the schematic diagram of band edge positions.

Sample structure	Secondary electron cutoff (eV, KE, work function)	VB to Fermi Level (eV, BE)	Ionization potential (eV)
glass/ITO/poly-TPD	4.61	0.46	5.07
	4.55	0.43	4.99
	4.60	0.39	4.99
	4.67	0.40	5.07
Average	4.61	0.42	5.03
glass/ITO/poly-TPD/2PACz	5.15	0.75	5.89
	5.11	0.77	5.88
	5.22	0.80	6.02
	5.18	0.80	5.98
Average	5.16	0.78	5.94
glass/ITO/poly-TPD/2PACz/ perovskite	4.39	1.74	6.12
	4.38	1.74	6.11
	4.36	1.75	6.11
	4.63	1.16	5.78
Average	4.44	1.59	6.03
glass/ITO/poly-TPD/2PACz/ perovskite/HO-PEAI	4.07	2.02	6.09
	4.06	1.96	6.02
	4.08	1.96	6.04
	4.25	1.50	5.75
	4.09	2.01	6.10
Average	4.11	1.89	6.00
glass/ITO/poly-TPD/2PACz/ perovskite/2-TEAI	3.97	2.19	6.16
	3.92	2.18	6.10
	3.96	2.21	6.16
	4.03	2.02	6.05
	4.06	2.07	6.14
Average	3.99	2.14	6.12
glass/ITO/poly-TPD/2PACz/ Perovskite/ PCBM	4.91	0.75	5.66
	4.91	0.73	5.65
	4.96	0.68	5.64
	5.07	0.56	5.63
	4.96	0.72	5.68
Average	4.96	0.69	5.65
glass/ITO/poly-TPD/2PACz/ Perovskite/HO-PEAI/ PCBM	5.00	0.61	5.60
	5.06	0.65	5.71
	5.07	0.64	5.71
	4.74	0.94	5.68
	5.08	0.64	5.72
Average	4.99	0.70	5.69
glass/ITO/poly-TPD/2PACz/ Perovskite/2-TEAI/ PCBM	5.04	0.64	5.68
	5.06	0.64	5.70
	5.06	0.66	5.72
	5.06	0.65	5.71
	5.06	0.67	5.73
Average	5.06	0.66	5.71

Table S5. The photovoltaic parameters of devices with the structure of glass/ITO/poly-TPD/2PACz/perovskite/2-TEAI/PCBM/BCP/Ag. The devices were measured outside the glove box under simulated AM 1.5G solar irradiation at 100 mW cm^{-2}. For each device, the *J-V* curves were only scanned once, consisting of the forward scan (FS, – 0.2 to 1.2 V) and reverse scan (RS, 1.2 to – 0.2 V).

Device	Scan direction	V_{OC} (V)	J_{SC} (mA cm^{-2})	FF	PCE (%)	Device	Scan direction	V_{OC} (V)	J_{SC} (mA cm^{-2})	FF	PCE (%)
1	RS	1.16	21.70	0.81	20.50	22	RS	1.18	20.74	0.82	19.92
	FS	1.16	21.61	0.82	20.44		FS	1.18	20.67	0.81	19.72
2	RS	1.20	20.66	0.82	20.39	23	RS	1.18	21.01	0.81	20.07
	FS	1.20	20.58	0.81	20.14		FS	1.18	20.99	0.81	19.99
3	RS	1.18	21.32	0.80	20.15	24	RS	1.19	20.95	0.81	20.26
	FS	1.18	21.26	0.80	20.18		FS	1.19	20.93	0.81	20.22
4	RS	1.19	20.89	0.83	20.59	25	RS	1.18	21.30	0.81	20.35
	FS	1.18	20.77	0.81	19.86		FS	1.18	21.27	0.80	20.22
5	RS	1.19	20.84	0.83	20.43	26	RS	1.17	22.05	0.80	20.71
	FS	1.19	20.69	0.82	20.19		FS	1.17	22.04	0.80	20.61
6	RS	1.19	21.16	0.82	20.70	27	RS	1.18	22.12	0.82	21.40
	FS	1.19	21.16	0.82	20.58		FS	1.18	22.13	0.81	21.25
7	RS	1.18	20.34	0.82	19.75	28	RS	1.18	21.13	0.81	20.14
	FS	1.18	20.27	0.81	19.43		FS	1.17	21.05	0.81	20.03
8	RS	1.19	21.92	0.82	21.35	29	RS	1.20	21.93	0.83	21.92
	FS	1.18	21.83	0.83	21.40		FS	1.20	22.09	0.83	21.85
9	RS	1.17	21.77	0.83	21.09	30	RS	1.17	20.47	0.83	19.85
	FS	1.17	21.82	0.82	20.98		FS	1.17	20.44	0.83	19.74
10	RS	1.18	21.88	0.83	21.42	31	RS	1.17	21.26	0.83	20.57
	FS	1.19	21.80	0.82	21.27		FS	1.17	21.26	0.83	20.49
11	RS	1.19	21.82	0.82	21.21	32	RS	1.17	20.63	0.83	20.08
	FS	1.19	21.80	0.82	21.41		FS	1.17	20.51	0.83	19.79
12	RS	1.19	21.79	0.83	21.53	33	RS	1.19	20.80	0.83	20.62
	FS	1.18	21.67	0.83	21.19		FS	1.19	20.73	0.82	20.31
13	RS	1.19	22.31	0.83	21.95	34	RS	1.18	21.22	0.82	20.66
	FS	1.18	22.28	0.83	21.79		FS	1.18	21.16	0.82	20.59
14	RS	1.20	21.16	0.80	20.35	35	RS	1.18	20.91	0.83	20.41
	FS	1.20	21.11	0.81	20.39		FS	1.18	20.95	0.82	20.31
15	RS	1.18	22.00	0.83	21.54	36	RS	1.18	21.53	0.83	20.95
	FS	1.18	21.97	0.83	21.36		FS	1.18	21.50	0.82	20.71
16	RS	1.18	22.25	0.82	21.61	37	RS	1.19	20.55	0.82	20.13
	FS	1.18	22.26	0.82	21.50		FS	1.19	20.46	0.82	20.00
17	RS	1.19	20.97	0.82	20.55	38	RS	1.18	21.22	0.83	20.89
	FS	1.19	20.84	0.82	20.18		FS	1.19	21.14	0.82	20.53
18	RS	1.18	21.19	0.83	20.69	39	RS	1.16	22.28	0.83	21.42
	FS	1.18	21.14	0.82	20.30		FS	1.16	22.26	0.82	21.30
19	RS	1.18	20.86	0.80	19.80	40	RS	1.19	21.51	0.83	21.42
	FS	1.18	20.86	0.80	19.77		FS	1.19	21.41	0.83	21.25
20	RS	1.17	20.97	0.81	19.89	41	RS	1.19	21.48	0.84	21.36
	FS	1.17	20.89	0.81	19.68		FS	1.19	21.46	0.82	21.04
21	RS	1.17	21.09	0.82	20.18	42	RS	1.18	21.53	0.82	20.96
	FS	1.17	21.04	0.82	20.13		FS	1.19	21.55	0.81	20.83

Table S6. A summary of IPSCs based on the poly-TPD.

Device structure	V_{OC} **(V)**	J_{SC} **(mA cm^{-2})**	**FF**	**PCE (%)**	**Year**
glass/ITO/PEDOT:PSS/poly-TPD/$MAPbI_3$/PCBM/Au	1.05	16.12	0.67	12.04	2014[13]
glass/ITO/poly-TPD/$MAPbI_3$ (two-step)/PCBM/C_{60}/BCP/Ag	1.10	22.0	0.70	15.3	2014[14]
glass/FTO/poly-TPD/$MAPbI_3$/PCBM/BCP/Ag	1.10	22.4	0.78	19.1	2016[15]
glass/ITO/poly-TPD (UV-ozone)/$MAPbI_3$/C_{60}/BCP/Ag	1.04	23.20	0.75	18.19	2017[16]
glass/ITO/poly-TPD/PFN-Br/$MAPbI_3$/PCBM/Al	1.11	21.23	0.81	19.14	2017[17]
glass/ITO/poly-TPD (O_2 plasma)/$MAPbI_3$/C_{60}/BCP/Cu	1.03	21.4	0.75	16.5	2018[18]
glass/ITO/poly-TPD/PFN-Br/$MAPbI_3$/PCBM/LiF/Ag	1.07	21.8	0.74	17.2	2019[19]
glass/ITO/poly-TPD/PFN-Br/$Cs_{0.05}(MA_{0.17}FA_{0.83})_{0.95}Pb(I_{0.83}Br_{0.17})_3$/$C_{60}$/-BCP/Au	1.13	22.3	0.81	20.3	2019[20]
glass/FTO/poly-TPD/$Cs_{0.17}FA_{0.83}Pb(I_{0.90}Br_{0.10})_3$/PCBM/BCP/Cr/Au	1.12	22.8	0.79	20.1	2020[21]
glass/ITO/poly-TPD/PFN-I/$Cs_{0.05}MA_{0.16}FA_{0.79}PbI_{2.4}Br_{0.6}$/PFN-I/PCBM/BCP/Ag	1.13	22.48	0.81	20.56	2020[12]
glass/ITO/poly-TPD/PFN-Br/$Cs_{0.05}MA_{0.16}FA_{0.79}PbI_{2.4}Br_{0.6}$/PEAI/PCBM/BC-P/Ag	1.18	21.86	0.83	21.33	2020[3]
glass/ITO/poly-TPD/PFN-Br/$Cs_{0.05}MA_{0.16}FA_{0.79}PbI_{2.4}Br_{0.6}$/PMAI/PCBM/BC-P/Ag	1.17	22.42	0.82	21.51	2020[3]
glass/ITO/poly-TPD/2PACz/$Cs_{0.05}MA_{0.16}FA_{0.79}PbI_{2.4}Br_{0.6}$/2-TEAI/PCBM/BCP/Ag	1.20	22.09	0.83	21.92	This work

References

[1] S. Bai, P. Da, C. Li, Z. Wang, Z. Yuan, F. Fu, M. Kawecki, X. Liu, N. Sakai, J. T. W. Wang, S. Huettner, S. Buecheler, M. Fahlman, F. Gao, H. J. Snaith, *Nature* **2019**, *571*, 245.

[2] D. Luo, W. Yang, Z. Wang, A. Sadhanala, Q. Hu, R. Su, R. Shivanna, G. F. Trindade, J. F. Watts, Z. Xu, T. Liu, K. Chen, F. Ye, P. Wu, L. Zhao, J. Wu, Y. Tu, Y. Zhang, X. Yang, W. Zhang, R. H. Friend, Q. Gong, H. J. Snaith, R. Zhu, *Science.* **2018**, *360*, 1442.

[3] B. Li, Y. Xiang, K. D. G. I. Jayawardena, D. Luo, Z. Wang, X. Yang, J. F. Watts, S. Hinder, M. T. Sajjad, T. Webb, H. Luo, I. Marko, H. Li, S. A. J. Thomson, R. Zhu, G. Shao, S. J. Sweeney, S. R. P. Silva, W. Zhang, *Nano Energy* **2020**, *78*, 105249.

[4] M. Anaya, B. P. Rand, R. J. Holmes, D. Credgington, H. J. Bolink, R. H. Friend, J. Wang, N. C. Greenham, S. D. Stranks, *Nat. Photonics* **2019**, *13*, 818.

[5] B. L. Henke, E. M. Gullikson, J. C. Davis, *At. Data Nucl. Data Tables* **1993**, *54*, 181.

[6] G. Ashiotis, A. Deschildre, Z. Nawaz, J. P. Wright, D. Karkoulis, F. E. Picca, J. Kieffer, *J. Appl. Crystallogr.* **2015**, *48*, 510.

[7] G. Kresse, J. Furthmüller, *Comput. Mater. Sci.* **1996**, *6*, 15.

[8] J. P. Perdew, K. Burke, M. Ernzerhof, *Phys. Rev. Lett.* **1997**, *78*, 1396.

[9] G. Kresse, D. Joubert, *Phys. Rev. B* **1999**, *59*, 1758.

[10] H. J. Monkhorst, J. D. Pack, *Phys. Rev. B* **1976**, *13*, 5188.

[11] U. Rau, *Phys. Rev. B* **2007**, *76*, 85303.

[12] B. Li, Y. Xiang, K. D. G. I. Jayawardena, D. Luo, J. F. Watts, S. Hinder, H. Li, V. Ferguson, H. Luo, R. Zhu, S. R. P. Silva, W. Zhang, *Sol. RRL* **2020**, 2000060.

[13] O. Malinkiewicz, A. Yella, Y. H. Lee, G. M. Espallargas, M. Graetzel, M. K. Nazeeruddin, H. J. Bolink, *Nat. Photonics* **2013**, *8*, 128.

[14] D. Zhao, M. Sexton, H. Y. Park, G. Baure, J. C. Nino, F. So, *Adv. Energy Mater.* **2014**, *5*, 1401855.

[15] J. T. W. Wang, Z. Wang, S. Pathak, W. Zhang, D. W. deQuilettes, F. Wisnivesky-Rocca-Rivarola, J. Huang, P. K. Nayak, J. B. Patel, H. A. Mohd Yusof, Y. Vaynzof, R. Zhu, I. Ramirez, J. Zhang, C. Ducati, C. Grovenor, M. B. Johnston, D. S. Ginger, R. J. Nicholas, H. J. Snaith, *Energy Environ. Sci.* **2016**, *9*, 2892.

[16] X. Xu, C. Ma, Y. Cheng, Y. M. Xie, X. Yi, B. Gautam, S. Chen, H. W. Li, C. S. Lee, F. So, S. W. Tsang, *J. Power Sources* **2017**, *360*, 157.

[17] J. Lee, H. Kang, G. Kim, H. Back, J. Kim, S. Hong, B. Park, E. Lee, K. Lee, *Adv. Mater.* **2017**, *29*, 1606363.

[18] S. Zhang, M. Stolterfoht, A. Armin, Q. Lin, F. Zu, J. Sobus, H. Jin, N. Koch, P. Meredith, P. L. Burn, D. Neher, *ACS Appl. Mater. Interfaces* **2018**, *10*, 21681.

[19] H. K. H. Lee, J. Barbé, S. M. P. Meroni, T. Du, C. T. Lin, A. Pockett, J. Troughton, S. M. Jain, F. De Rossi, J. Baker, M. J. Carnie, M. A. McLachlan, T. M. Watson, J. R. Durrant, W. C. Tsoi, *Sol. RRL* **2019**, *3*, 1800207.

[20] M. Stolterfoht, P. Caprioglio, C. M. Wolff, J. A. Márquez, J. Nordmann, S. Zhang, D. Rothhardt, U. Hörmann, Y. Amir, A. Redinger, L. Kegelmann, F. Zu, S. Albrecht, N.

Koch, T. Kirchartz, M. Saliba, T. Unold, D. Neher, *Energy Environ. Sci.* **2019**, *12*, 2778-2788.

[21] Y. H. Lin, N. Sakai, P. Da, J. Wu, H. C. Sansom, A. J. Ramadan, S. Mahesh, J. Liu, R. D. J. Oliver, J. Lim, L. Aspitarte, K. Sharma, P. K. Madhu, A. B. Morales-Vilches, P. K. Nayak, S. Bai, F. Gao, C. R. M. Grovenor, M. B. Johnston, J. G. Labram, J. R. Durrant, J. M. Ball, B. Wenger, B. Stannowski, H. J. Snaith, *Science.* **2020**, *369*, 96.